## ABSTRACT

## RESOURCE ALLOCATION, USER ASSOCIATION AND PLACEMENT FOR UAV-ASSISTED COMMUNICATIONS

by
**Shuai Zhang**

In the past few years, unmanned aerial vehicle (UAV)-assisted heterogeneous network has attracted significant attention due to its wide range of applications, such as disaster rescue and recovery, ground macro base station (MBS) traffic offloading, communications for temporary events, and data collection for further processing in Internet of Things (IoT). A UAV can act as a flying base station (BS) to quickly recover the communication coverage in the disaster area when the regular terrestrial infrastructure is malfunctioned. The UAV-assisted heterogeneous network can effectively provision line of sight (LoS) communication links and therefore can mitigate potential signal shadowing and blockage. The regulation relaxation and cost reduction of UAVs as well as communication equipment miniaturization make the practical deployment of highly mobile wireless relays more feasible than before. In fact, the 3GPP Rel-16 has included UAV-enabled wireless communications in the new radio standard, aiming to boost capacity and coverage of fifth generation (5G) wireless networks. However, the performance of UAV-assisted communications is greatly affected by the resource allocation scheme, user association policy and the UAV placement strategy. Also, the limited on-board energy and flight time of the UAV poses a great challenge on designing a robust and reliable UAV-enabled IoT network.

To maximize the throughput in the UAV-assisted mobile access network, an optimization problem which determines the 3D UAV deployment and resource allocation in a given hotspot area under the constraints of user Quality of Service (QoS) requirements and total available resources is formulated. First, the primal

problem is decomposed into two subproblems, i.e., the 3D UAV placement problem and the resource allocation problem. Second, a cyclic iterative algorithm which solves the two sub-problems separately and uses the output of one as the input of the other is proposed.

An optimization problem that aims to minimize the average latency ratio of all users is formulated by determining the 3D location of the UAV, the user association and the bandwidth allocation policy between the MBS and the drone base station (DBS) with the constraint of each user's QoS requirement and total available bandwidth. The formulated problem is a mixed integer non-convex optimization problem, a very challenging and difficult problem. To make formulated problem tractable, it is decomposed into two subproblems, i.e., the user association and bandwidth allocation problem and the 3D DBS placement problem. These two subproblems are alternatively optimized until no performance improvement can be further achieved.

To address the challenge of limited on-board battery capacity and flight time, a tethered UAV (TUAV)-assisted heterogeneous network where the aerial UAV is connected with a ground charging station (GCS) through a tether is proposed. The objective of the formulated problem is to maximize the sum rate of all users by jointly optimizing the user association, resource allocation and placement of the GCSs and the aerial UAVs, constrained by each user's QoS requirement and the total available resource. Since the primal problem is highly non-convex and non-linear and thus challenging to solve, it is decomposed into three subproblems, i.e., the TUAV placement problem, the resource allocation problem and the user association problem. Then, the three sub-problems are alternately and iteratively optimized by using the outputs of the first two as the input for the third.

The future work comprises two parts. First, IoT devices usually are generally deployed at remote areas with limited battery capacities and computing power.

Therefore, the generated data needs to be offloaded to a more powerful computing server for further processing. Unfortunately, the trajectory design in UAV data collection is generally NP-hard and difficult to obtain the optimal solution. Advances of machine learning (ML) provide a promising alternative approach to solve such problems that cannot be solved by traditional optimization methods. Hence, deep reinforcement learning (DRL) is proposed to be explored to obtain a near optimal solution. Second, the low earth orbit (LEO) satellite networks will revolutionize traditional communication networks with their promising benefits of service continuity, wide-area coverage, and availability for critical communications and emerging applications. However, the integration of LEO satellite networks and terrestrial networks will be another future research endeavor.

# RESOURCE ALLOCATION, USER ASSOCIATION AND
# PLACEMENT FOR UAV-ASSISTED COMMUNICATIONS

by
Shuai Zhang

A Dissertation
Submitted to the Faculty of
New Jersey Institute of Technology
in Partial Fulfillment of the Requirements for the Degree of
Doctor of Philosophy in Electrical Engineering

Helen and John C. Hartmann Department of
Electrical and Computer Engineering

August 2022

# RESOURCE ALLOCATION, USER ASSOCIATION AND PLACEMENT FOR UAV-ASSISTED COMMUNICATIONS

## Shuai Zhang

Dr. Nirwan Ansari, Dissertation Advisor                                    Date
Distinguished Professor, Helen and John C. Hartmann Department of
Electrical and Computer Engineering, NJIT


Dr. Roberto Rojas-Cessa, Committee Member                          Date
Professor, Helen and John C. Hartmann Department of
Electrical and Computer Engineering, NJIT


Dr. Abdallah Khreishah, Committee Member                          Date
Associate Professor, Helen and John C. Hartmann Department of
Electrical and Computer Engineering, NJIT


Dr. Qing Liu, Committee Member                                        Date
Associate Professor, Helen and John C. Hartmann Department of
Electrical and Computer Engineering, NJIT


Dr. Jing Li, Committee Member                                          Date
Assistant Professor, Department of Computer Science, NJIT

# BIOGRAPHICAL SKETCH

**Author:**           Shuai Zhang

**Degree:**          Doctor of Philosophy

**Date:**             August 2022

## Undergraduate and Graduate Education:

- Doctor of Philosophy in Electrical Engineering,
  New Jersey Institute of Technology, Newark, NJ, 2022.

- Master of Engineering in Signal and Information Processing,
  University of Electronic Science and Technology of China, Chengdu, China,
  2017.

- Bachelor of Engineering in Electronic Information Engineering,
  University of Electronic Science and Technology of China, Chengdu, China,
  2014.

**Major:**             Electrical Engineering

## Presentations and Publications:

**S. Zhang**, W. Liu and N. Ansari, "Joint Wireless Charging and Data Collection for UAV-enabled Internet of Things Network," *IEEE Internet of Things Journal*, (Early access).

**S. Zhang**, W. Liu and N. Ansari, "On Tethered UAV-Assisted Heterogeneous Network," *IEEE Transactions on Vehicular Technology*, vol. 71, no. 1, pp. 975-983, Jan. 2022.

**S. Zhang** and N. Ansari, "Latency Aware 3D Placement and User Association in Drone-Assisted Heterogeneous Networks With FSO-Based Backhaul," *IEEE Transactions on Vehicular Technology*, vol. 70, no. 11, pp. 11991-12000, Nov. 2021.

**S. Zhang** and N. Ansari, "3D Drone Base Station Placement and Resource Allocation With FSO-Based Backhaul in Hotspots," *IEEE Transactions on Vehicular Technology*, vol. 69, no. 3, pp. 3322-3329, March 2020.

W. Liu, **S. Zhang** and N. Ansari, "Joint Laser Charging and DBS Placement for Drone-Assisted Edge Computing," *IEEE Transactions on Vehicular Technology*, vol. 71, no. 1, pp. 780-789, Jan. 2022.

**S. Zhang**, X. Sun and N. Ansari, "Placing Multiple Drone Base Stations in Hotspots," *IEEE 39th Sarnoff Symposium*, 2018, pp. 1-6.

*Advancing Technology for Humanity.*

# ACKNOWLEDGMENT

# LIST OF TABLES

# LIST OF FIGURES

# CHAPTER 1

# INTRODUCTION

Recently, unmanned aerial vehicle (UAV)-assisted heterogeneous network has attracted significant attention due to its wide range of applications, such as disaster rescue and recovery, aerial camera, ground macro base station (MBS) traffic offloading [1], and communications for temporary events [2]. The UAV-assisted heterogeneous network can effectively provision line of sight (LoS) communication links [3] and therefore can mitigate potential signal shadowing and blockage. The regulation relaxation and cost reduction of UAVs as well as communication equipment miniaturization make the practical deployment of highly mobile wireless relays more feasible than before. In fact, the 3GPP Rel-16 has included UAV-enabled wireless communications in the new radio standard, aiming to boost capacity and coverage of existing wireless networks [4]. Meanwhile, the approval of Federal Aviation Administration (FAA) paves the way to a large-scale deployment of UAV-enabled heterogeneous wireless networks, especially for on-demand application scenarios.

In a UAV-assisted wireless network, there are several challenging issues need to be addressed. The backhaul capacity should be high enough to support the traffic transmitted from the MBS. Since the total available bandwidth is limited, an inband backhaul approach may cause severe interference between the access link and the backhaul link (i.e., in-band-full-duplex method) or decrease the available bandwidth in each link (i.e., inband-half-duplex method). Therefore, it is critical to properly design the resource allocation scheme to maximize the system throughput or minimize the system latency. Free Space Optics (FSO), with its potential high capacity, can be utilized to build the connection between the UAV and the MBS (i.e., the backhaul link). It has been demonstrated that FSO links can achieve a data rate of 1–2 Gbps

over distances in the range of 1–5 km [5–8]. In the meantime, employing FSO in the backhaul link [9, 10] will not cause interference or decrease the available bandwidth (because FSO works on a frequency range different from the radio frequency signal) in the access link. In addition, the operating time of the UAV is greatly constrained by the limited on-board energy. The current state-of-art UAVs can only stay in the air for less than one hour before battery depletion [11]. The hovering time is further reduced with consideration of the energy consumption for the payload, communication and signal processing. Therefore, a stable power supply needs to be provided to enable the UAV to stay in the air for a longer time.

First, deploying a UAV over a given area with FSO-based backhaul can significantly improve the Quality of Service (QoS) of users and increase the system throughput. Note that the 3D location of the UAV not only influences the user QoS in the access link but also affects the capacity of the FSO link. To satisfy the user QoS requirements and maximize the throughput of the access link, the UAV should be placed as close to the given area as possible. However, moving the UAV close to the given area increases the distance between the FSO transmitter and receiver. The increase of such distance leads to the decrease of the received power, and the capacity of the backhaul link will thus be reduced. Therefore, the UAV should be properly placed to satisfy the user QoS requirements as well as to provision a large capacity in the backhaul link to support the traffic aggregated in the access link. The limited available bandwidth and power should also be optimized in the access link to further improve the system throughput. Additionally, the pathloss of each user is decided by the 3D location of the UAV; a different placement policy of the UAV will result in a different resource allocation scheme. In conclusion, the placement of the UAV and resource allocation policy should be jointly considered. We design a Cyclic Iterative UAV placEment and Resource allocation (CIDER) algorithm to maximize the throughput of the access link while satisfying the user QoS requirements.

Second, deploying a UAV in an existing cellular network can also help reduce the network latency. However, it must overcome the following challenges: 1) How to determine the location of the UAV? The deployment of the UAV not only affects the user QoS but also influences the association policy (i.e., whether a user should be associated with the MBS or the UAV). For users associated with the UAV, moving the UAV closer to one user may decrease its latency ratio (i.e., the amount of time a user must be sacrificed in waiting for a unit service time) but at the expense of the latency ratio of another user. Therefore, the location of the UAV should be optimized to minimize the overall latency ratio while satisfying the user QoS requirements. 2) What is the association policy of the users? Associating with an access point which has a better channel condition (i.e., a lower pathloss) will increase the data rate. Intuitively, more users should be associated with the UAV since an LoS communication link is more likely to be established between the UAV and a user. However, too many users associating with the UAV may increase the traffic load and thus significantly increase the latency ratio of the users. Therefore, it is necessary to properly design the user association policy to minimize the overall latency ratio. 3) What is the optimal bandwidth allocation scheme between the MBS and UAV? Allocating more bandwidth to the MBS or UAV will decrease the latency ratio of its associated users; however, the latency ratio of users which are not associated with the access point will increase (less bandwidth becomes available for them). Meanwhile, the placement of the UAV, the user association policy and the bandwidth allocation scheme are mutually dependent. As a result, the three subproblems mentioned above should be jointly considered to minimize the overall latency ratio. To tackle the above challenges, we propose to decompose the joint optimization problem into two subproblems, i.e., the user association and bandwidth allocation problem and the UAV placement problem, to minimize the overall latency ratio.

Third, to enable the UAVs to stay in the air for a longer time, we can consider to increase the UAV's battery capacity. However, the lithium-ion battery (which is widely used) energy density is expected to achieve a steady 3% performance increase per year, meaning that it takes roughly 24 years to double the capacity of current battery (i.e., double the flight time of a UAV from 30 minutes to 1 hour). Even though the capacity is doubled, it is still not enough to provide continuous service to a typical temporary event, which usually lasts several hours. All those factors mentioned above preclude improving the battery capacity as a solution to solving the problem of UAV's limited on-board energy [12]. Wireless Power Transfer (WPT) could be a promising solution [13]. Two techniques, i.e., electromagnetic field (EMF) charging and non-EMF charging, are adopted for WPT. Specifically, the EMF charging uses electro-magnetic fields to wirelessly charge the target battery. Unfortunately, these techniques suffer from low energy transferring efficiency and thus cannot provide enough energy to compensate for that consumed by the UAV. Non-EMF charging employs high-power lasers [14,15] and photo-voltaic (PV) cells (which is mounted on the UAVs) to charge UAVs. The difficulty of using lasers and PV cells for energy transmission is that the transfer performance can be significantly degraded by bad weather conditions. Moreover, the receiver side may suffer from severe alignment errors because of the random fluctuation of the position and orientation of the UAVs. As a result, the amount of energy that the PV panel can collect will be dramatically reduced or diminished. Besides all the methods mentioned above, the most practical solution to prolong UAV's flight time is to connect the UAV through a tether with a ground charging station (GCS). The GCS can provide a stable power supply and a wired backhaul link (when Internet is accessible for the GCS) while maintaining UAV's maneuverability to a certain extent. Owing to the great potential of tethered UAV (TUAV), many well-known companies have started to test TUAVs, such as AT&T's "Flying Cell-On Wings (COWS)," Facebook's "tether-Tenna," and EE's

4

(EE is U.K.'s largest cellular operator) "Air Masts" [16]. As compared with deploying untethered UAVs, the following challenges need to be tackled: 1) How does one avoid not only the tangling between a TUAV and the surrounding buildings, but also the tangling among TUAVs? Deploying multiple TUAVs over a given area may cause tangling among them if two GCSs are placed at a distance which is shorter than the sum of the tether lengths. In addition, the inclination angle of each tether should be high enough to avoid tangling with the surrounding buildings. Note that the minimum allowed inclination angle is coupled with the placement of TUAVs, i.e., a different minimum allowed inclination angle will result in a different placement policy. Therefore, the minimum allowed inclination angles and the locations of TUAvs should be jointly considered to maximize the sum rate in the access link. 2) What are the optimal locations of the GCSs and UAVs? Considering the tether length, inclination angle and tangling avoidance constraint, the GCS cannot be placed at an arbitrary horizontal location. The location of the UAV is also constrained by the location of the corresponding GCS since they are connected via a tether. Therefore, it is necessary to properly determine the locations of GCSs and UAVs to prevent tangling and ensure safety. To address the above challenges, we propose a Cyclic iterAtive TUAV placeMent, usEr association and Resource Allocation (CAMERA) algorithm to maximize the sum rate in the access link with the constraints of limited available resource, tangling avoidance and user QoS requirements.

# CHAPTER 2

# RELATED WORKS

UAVs can be classifed into two main categories: rotary wing and fxed wing. A rotary wing UAV can theoretically hover at a fxed location while a fxed wing UAV has to maintain a minimum speed to stay aloft in the air. However, a rotary wing UAV generally consumes more energy and has less on-board energy as compared with a fxed-wing UAV. Various works have addressed the deployment of rotary wing UAVs in mobile networks. Al-Hourani *et al.* [3] derived the optimal altitude of a UAV, which is a function of the maximum pathloss allowance between a user and the UAV, in order to maximize the coverage area of the UAV. Kalantari *et al.* [17] proposed a UAV placement algorithm to maximize the number of covered users in the constrained backhauling scenario (i.e., the backhaul link may also be the bottleneck in downloading traffic from the MBS to a user). Mozaffari *et al.* [1] proposed to apply a UAV to facilitate Device-to-Device (D2D) communications. Here, the UAV is considered as a mobile intermediate node to relay D2D traffic from the source user to the destination user. They designed a method to minimize the number of the stop points that the UAV needs to visit in order to enable the UAV completely cover the whole area. Liu and Ansari [18] proposed a UAV network access and resource allocation scheme to maximize the number of human portable/wearable Machine Type Dvices (MTDs). Their simulations showed that the proposed scheme can achieve a higher spectrum efficiency and cover a larger number of MTDs.

There are also extensive works studying the deployment of fixed wing UAVs. Due to its larger on-board energy and longer flight time, fixed wing UAVs can be used to collect data of devices which are deployed in sparse areas and provide wireless energy by utilizing Wireless Power Transfer (WPT). Zeng *et al.* [19] proposed to

deploy a UAV to work as a mobile relay between the transmitter and receiver. The transmit power and the trajectory of the UAV are optimized to achieve the highest data rate between the source node and the target node while considering the constraint of the UAV's maximum speed. Xie *et al.* [20] proposed to dispatch a UAV to periodically charge and serve the ground users by utilizing WPT. They aimed to maximize the minimum data rate in the uplink with the constraints of the UAV's maximum speed and the users' power budget. However, they assumed the transmit power in the downlink WPT to be constant, which may increase the energy consumption of the UAV and therefore reduce the time remaining in the air. Zhan *et al.* [21] studied the minimization of energy consumption and completion time of the fixed wing UAV-enabled mobile edge computing (MEC) system for IoT computation offloading. Fadlullah *et al.* [22,23] proposed to deploy a number of UAVs to facilitate network communication. They proposed effective dynamic trajectory control algorithm and efficient time-slot allocation scheme to increase the throughput, reduce the delay and mitigate the interference among UAVs.

Modeling the FSO channel has been extensively studied. Most works focus on the quantization of the pathloss and potential capacity, which are determined by the weather conditions, system parameters (such as transmission power, frequency and efficiency etc.) and transmitting distance. Najafi *et al.* [24] proposed to place drone base station (DBS) over a hotspot area and to employ FSO links for fronthauling of user data to a central unit. The geometric loss of the FSO channel caused by the drone's instability and the non-orthogonality of the laser beam with respect to the photodetector plane is quantified. Alzenad *et al.* [25] investigated a novel backhaul/fronthaul framework in 5G+ wireless networks where the DBS transports the backhaul/fronthaul traffic between the access and the core networks through FSO links. They demonstrated via simulations that their proposed FSO-based vertical backhaul/fronthaul framework can achieve higher data rates

than the baseline alternatives. Farid and Hranilovic [26] studied the performance of FSO communication links over slow fading channels from an information theory perspective, and they derived a statistical model which describes the received optical intensity fluctuation and pointing errors.

Works related to TUAV deployment in the existing literature are very limited. Kishk *et al.* [27] studied the optimal placement of TUAVs given the tether length and the height of the surround buildings to avoid tangling and ensure safety. However, they only focused on deploying one TUAV and did not consider the resource allocation scheme and user association policy. In [28], tethered balloons work as relays among multiple high altitude platform drones and ground stations to assist the existing cellular network. In [29] , tethered balloons are used to establish backhaul links among the multiple UAVs and ground users to recover communications in an infrastructure-less environment. Pai and Sainath [30] proposed to deploy tethered UAV to assist the existing base station to improve the end-to-end performance, and they analyzed the outage probability of their proposed policy.

The rest of this thesis is organized as follows. In Chapter 3, the architecture of a DBS assisted network is proposed. In the architecture, a DBS is deployed to d to act as a relay node between the users and the MBS to increase the system throughput. To support the heavy traffic in the access link, FSO is proposed to work as the backhaul link. In Chapter 4, a DBS-assisted heterogeneous network which helps reduce the user latency is proposed. By offloading traffic to the DBS which provides a better channel condition, the user latency can be significantly reduced. The optimization problem is formulated to minimize the average latency ratio of all users subject to the user QoS requirements and limited available bandwidth. In Chapter 5, the deployment of multiple tethered UAVs to help provide service to the ground users is investigated. Connecting with ground charging station through a tether, the lifetime of a UAV can be greatly extended by replacing the charging box when necessary while maintaining

UAV's maneuverability to a certain extent. Different from placing untethered UAVs, placing multiple TUAVs should avoid the tangling with surround buildings or the tangling among themselves to ensure safety. In addition, the placement of TUAVs includes not only the placement of the UAVs but also that of the ground charging base stations. Moreover, these two problems are constrained by the length of the tether. To solve this challenge, we try to determine the placement of the ground charging stations first and optimize the placement of the UAVs with the constraints of the tether length and tangling avoidance. A briefly presentation of the future research endeavors is introduced in Chapter 6. The conclusion is presented in Chapter 7.

# CHAPTER 3

# THROUGHPUT MAXIMIZATION
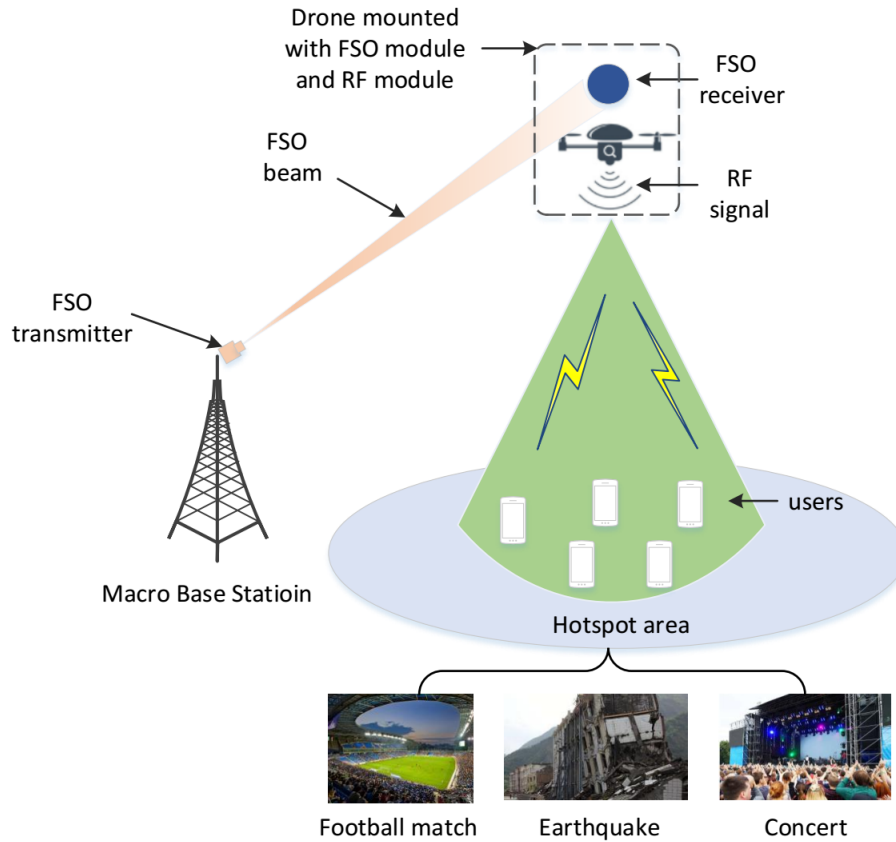


**Figure 3.1** DBS-assisted mobile access network.

As shown in Figure 3.1, we consider a hotspot area in which a large number of users are requesting high-data-rate downlink communications. In this area, a drone base station (DBS) is deployed to act as a relay node between the users and the MBS. In the access link, an orthogonal spectrum sharing scheme is employed to avoid the interference between the users. In the backhaul link, FSO is adopted to provide high capacity. The interference between the access link and backhual link can be ignored as they are operating in separate bands. The hotspot users are assumed to be located

uniformly in the hotspot area with density $\phi$ (number of users per m$^2$). Denote the set of users as $\mathcal{I} = \{1, 2, ..., I\}$. We summarize all the notations in Table 3.1.

**Table 3.1** Summary of Notations

| Notation | Definition |
|---|---|
| $a, b$ | Environment parameters. |
| $c$ | Speed of light. |
| $C$ | Data rate of the FSO link. |
| $f$ | Carrier frequency. |
| $x$ | Longitude of the DBS. |
| $y$ | Latitude of the DBS. |
| $h$ | Altitude of the DBS. |
| $r_i$ | Horizontal distance between user $i$ and the DBS. |
| $d_i$ | 3D distance between user $i$ and the DBS. |
| $\theta_i$ | Elevation angle between user $i$ and the DBS. |
| $P_i^{LoS}$ | Probability of an LoS connection between user $i$ and DBS. |
| $P_i^{NLoS}$ | Probability of an NLoS connection between user $i$ and DBS. |
| $\eta_{LoS}$ | Average excessive pathloss of an LoS connection. |
| $\eta_{NLoS}$ | Average excessive pathloss of an NLoS connection. |
| $\xi_i$ | Average pathloss between user $i$ and the DBS. |
| $\beta_i$ | Bandwidth allocated to user $i$ by the DBS. |
| $P_i$ | Transmission power allocated to user $i$ by the DBS. |
| $n_0$ | Noise power spectral density. |
| $T_i$ | Data rate requirement of user $i$. |
| $\phi_i$ | Pathloss requirement of user $i$. |

### 3.1  Downlink System Model

In this section, we first present the pathloss model of the access link and furthermore derive the data rate of each user. We then study the capacity of the FSO-based backhaul link. Finally, we formulate the optimization problem to maximize the throughput while satisfying the QoS requirement of all the users in the hotspot area. The constraint of the backhaul link is also being taken into consideration by setting the backhaul capacity larger than the throughput of the access link.

### 3.1.1  Data Rate Model in the Access Link

The wireless propagation channel between user $i$ and the DBS is modeled as a probabilistic LoS channel, and the probability of having an LoS connection between user $i$ and the DBS is [31, 32]

$$P_i^{LoS} = \frac{1}{1 + a \exp(-b(\frac{180}{\pi}\theta_i - a))}, \tag{3.1}$$

where $a$ and $b$ are the parameters determined by the surrounding environment of the users, and $\theta_i$ is the elevation angle between user $i$ and the DBS (i.e., $\theta_i = \arctan \frac{h}{r_i}$, where $h$ and $r_i$ are the altitude of the DBS and the horizontal distance between user $i$ and the DBS, respectively) as shown in Figure 3.2. Accordingly, the probability of having an NLoS connection is $P_i^{NLoS} = 1 - P_i^{LoS}$. Hence, the average pathloss between user $i$ and the DBS is [33]

$$
\begin{aligned}
\xi_i &= \mathcal{G}\left(\theta_i, r_i\right) \\
&= 20 \log\left(\frac{4\pi f d_i}{c}\right) + P_i^{LoS}\eta_{LoS} + P_i^{NLoS}\eta_{NLoS},
\end{aligned} \tag{3.2}
$$

where the first term is the free space pathloss (FSPL), $f$ is the carrier frequency, $c$ is the speed of light, $d_i$ is the 3D distance between user $i$ and the DBS and $d_i =$

$\sqrt{h^2 + r_i^2}$, and $\eta_{LoS}$ and $\eta_{NLoS}$ are the average excessive pathloss of having an LoS and NLoS connection between user $i$ and the DBS, respectively, where $\eta_{LoS} < \eta_{NLoS}$.
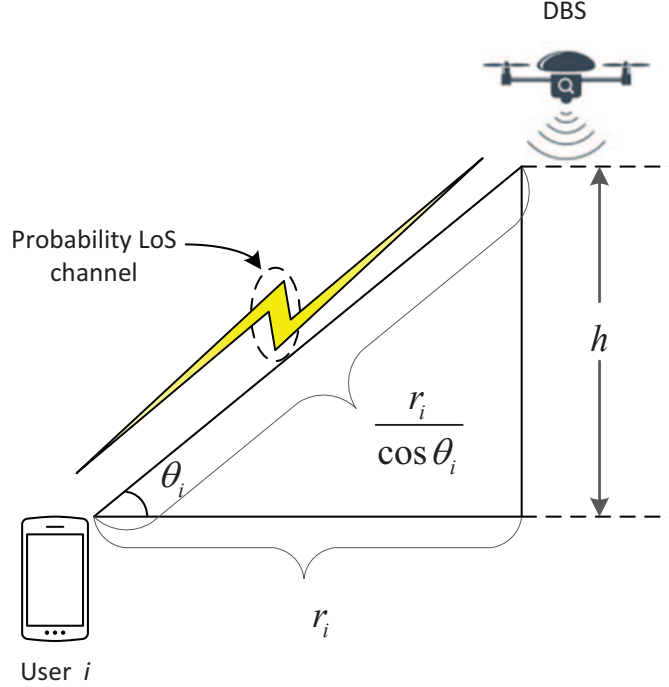


**Figure 3.2** The position of a DBS.

The data rate between user $i$ and the DBS can be derived based on the pathloss model shown in Equation (3.2) as

$$R_i = \beta_i \log_2(1 + \frac{P_i 10^{\frac{-\xi_i}{10}}}{n_0 \beta_i}),$$  (3.3)

where $\beta_i$ and $P_i$ are the bandwidth and transmission power allocated by the DBS for user $i$, respectively. $n_0$ is the noise power spectral density.

**Definition 1.** *The maximum horizontal distance between user $i$ and the DBS (denoted as $r_i^{max}$) is defined as the maximum value of $r_i$ such that the pathloss allowance of user $i$ still holds (i.e., $\mathcal{G}(\theta_i, r_i) \leq \phi_i$, where $\phi_i$ is the pathloss requirement).*

The horizontal distance between user $i$ and DBS can be maximized iff $\mathcal{G}\left(\theta_i, r_i\right) = \phi_i$, which is the function that defines the relationship between $\theta_i$ and $r_i$. In order to maximize $r_i$, we can take the derivative of $\mathcal{G}\left(\theta_i, r_i\right)$ with respect to $\theta_i$. By letting $\frac{\partial r_i}{\partial \theta_i} = 0$, we can derive the optimal elevation angle between user $i$ and DBS (that maximizes $r_i$) to be satisfied by the following equation [34, 35]:

$$\frac{\pi}{9\ln\left(10\right)}\tan\theta_i^* + \frac{ab\left(\eta_{LoS} - \eta_{NLoS}\right)\exp\left(-b\left(\frac{180}{\pi}\theta_i^* - a\right)\right)}{\left(a\exp\left(-b\left(\frac{180}{\pi}\theta_i^* - a\right)\right) + 1\right)^2} = 0, \tag{3.4}$$

where $\theta_i^*$ is the optimal elevation angle between user $i$ and DBS. By substituting $\theta_i = \theta_i^*$ into $\mathcal{G}\left(\theta_i, r_i\right) = \phi_i$, we can derive the maximum horizontal distance between user $i$ and DBS as

$$r_i^{max} = \frac{c\cos\theta_i^*}{4\pi f}10^{\frac{\phi_i - P_i^{LoS}\eta_{LoS} - P_i^{NLoS}\eta_{NLoS}}{20}}. \tag{3.5}$$

**Definition 2.** *The optimal altitude of the DBS with respect to user $i$ is defined as the altitude of DBS which incurs the maximum horizontal distance between user $i$ and DBS. That is, $h_i^* = r_i^{max}\tan(\theta_i^*)$, where $h_i^*$ is the optimal altitude of DBS with respect to user $i$.*

**Lemma 1.** *If the horizontal distance between user $i$ and DBS is $r_i^{max}$ and the altitude of DBS is $h_i^*$ (indicating that the elevation angle between user $i$ and DBS is $\theta_i^*$, and the pathloss between user $i$ and DBS just equals to user $i$'s pathloss requirement $\phi_i$), user $i'$, whose distance to the DBS is no larger than $r_i^{max}$ (i.e., $r_{i'} \leq r_i^{max}$) and pathloss requirement is no less than user $i$'s pathloss requirement (i.e., $\phi_{i'} \geq \phi_i$), can always meet its pathloss requirement (i.e., $\mathcal{G}\left(\theta_{i'}, r_{i'}\right) \leq \phi_{i'}$).*

*Proof.* Since $r_{i'} \leq r_i^{max}$ and the altitude of DBS is $h_i^*$, the elevation angle between user $i'$ and the DBS is no less than the elevation angle between user $i$ and DBS, i.e., $\theta_{i'} \geq \theta_i^*$, and thus the probability of having an LoS connection between user $i'$ and DBS should be no less than that of having an LoS connection between user $i$

14

and DBS, i.e., $P_{i'}^{LoS} \geq P_i^{LoS}$. Accordingly, we can derive that the average pathloss between user $i'$ and DBS should be no larger than that between user $i$ and DBS, i.e.,

$$\mathcal{G}\left(\theta_{i'}, r_{i'}\right) \leq \mathcal{G}\left(\theta_i^*, r_i^*\right). \tag{3.6}$$

Since the pathloss between user $i$ and DBS just equals to user $i$'s pathloss requirement $\phi_i$, i.e., $\mathcal{G}\left(\theta_i^*, r_i^*\right) = \phi_i$, we have

$$\mathcal{G}\left(\theta_{i'}, r_{i'}\right) \leq \phi_i \leq \phi_{i'}. \tag{3.7}$$

That is, user $i'$ can always meet its pathloss requirement. $\qquad\square$

### 3.1.2 Capacity Model of the FSO-based Backhaul Link

We adopt the data rate model presented in [5]:

$$C = \frac{P_t \eta_t \eta_r 10^{-\frac{L_{atm}}{10}} 10^{-\frac{L_{geo}}{10}}}{E_p N_b}, \tag{3.8}$$

where $P_t$ is transmission power, $\eta_t$ and $\eta_r$ denote the optical efficiencies of the transmitter and receiver, respectively; $E_p = h_p c / \lambda$ is the photon energy; $h_p$ denotes Plank's constant; $\lambda$ is the carrier wavelength; $N_b$ stands for the receiver sensitivity in number of photons/bit; $L_{geo}$ is the geometrical loss in dB given by $L_{geo} = 10 \log(\frac{\pi r^2}{\pi(\psi l/2)^2})$, $r$ is the radius of the receiver's aperture in m, $l$ is the distance between the laser transmitter and receiver in km, and $\psi$ denotes the transmitting divergence angle. $L_{atm}$ is the atmospheric attenuation caused by rain, fog, cloud or turbulence, which can be calculated by $L_{atm} = \frac{17}{V}(\frac{\lambda}{550nm})^{-q}$, where $L_{atm}$ is in dB/km, $V$ is the visibility in km, and $q$ is the size distribution of the scattering particles in different weather conditions. $q$ can be denoted as a function of the visibility distance [8]:

$$
q = \begin{cases}
1.6, & V > 50\,\text{km} \\[2ex]
1.3, & 6\,\text{km} < V \leq 50\,\text{km} \\[2ex]
0.16V + 0.34, & 1\,\text{km} < V \leq 6\,\text{km} \\[2ex]
V - 0.5, & 0.5\,\text{km} < V \leq 1\,\text{km} \\[2ex]
0, & V \leq 0.5\,\text{km}
\end{cases}
\tag{3.9}
$$

## 3.2 Problem Formulation

In this section, we formulate the optimization problem to maximize the aggregated data rate of all users in the hotspot area subject to their QoS requirements by jointly optimizing the DBS's location $x$, $y$, and $h$, bandwidth allocation $\beta_i$ and power allocation $P_i$ to each user. In our formulated problem, we try to determine both the DBS's 3D location (i.e., the longitude, latitude, and altitude) and the resource allocation scheme to each user at the same time. Meanwhile, we also take users' different QoS requirements (i.e., data rate requirements), limited available resource (i.e., power and bandwidth) and backhaul constraint (i.e., the capacity of the backhaul link should be larger than the throughput in the access link) into consideration. The problem can be formulated as

$$\textbf{P0: } \max_{x,y,h} \sum_{i=1}^{|\mathcal{I}|} R_i \tag{3.10}$$

$$s.t. \quad R_i \geq T_i, \forall i \in \mathcal{I}, \tag{3.11}$$

$$C \geq \sum_{i=1}^{|\mathcal{I}|} R_i \tag{3.12}$$

$$\sum_{i=1}^{|\mathcal{I}|} \beta_i = B, \tag{3.13}$$

$$\sum_{i=1}^{|\mathcal{I}|} P_i = P_{max}, \tag{3.14}$$

$$x^{min} \leq x \leq x^{max}, \tag{3.15}$$

$$y^{min} \leq y \leq y^{max}, \tag{3.16}$$

$$h^{min} \leq h \leq h^{max}, \tag{3.17}$$

$$\beta_i \geq 0, \forall i \in \mathcal{I}, \tag{3.18}$$

$$P_i \geq 0, \forall i \in \mathcal{I}, \tag{3.19}$$

where $T_i$ denotes the data requirement of user $i$, and $x$, $y$, and $h$ are the longitude, latitude, and altitude of the DBS, respectively. Variables $x_{min}$, $x_{max}$, $y_{min}$ and $y_{max}$ are the limits of the hotspot area. $h_{min}$ and $h_{max}$ denote the minimum and maximum altitude of a DBS allowed to reach, respectively. Constraint (3.11) indicates that the QoS requirement of each user should be satisfied. Constraint (3.12) implies that the backhaul capacity should be no less than the throughput in the access link. Constraints (3.13) and (3.14) stand for the resource limitations. Constraints (3.15), (3.16) and (3.17) are the 3D coordinates constraints of the DBS. Constraints (3.18) and (3.19) indicate that the bandwidth and power allocated to each user should be non-negative.

Unfortunately, **P0** is highly nonlinear and non-convex considering Equation (3.1) and Constraint (3.11). Next, we propose a Cyclic Iterative UAV placEment and Resource allocation (CIDER) algorithm to solve this optimization problem.

In essence, we decouple **P0** into two sub-problems. In each iteration, given the fixed DBS's location, we find the optimal bandwidth allocation and power allocation policy. Next, given the fixed resource allocation policy, we determine the suboptimal location of the DBS and update the aggregated data rate of all users accordingly. This procedure is done iteratively until the DBS's 3D location, bandwidth and power allocated to the users are found.

### 3.3   3D Drone Base Station Placement and Resource Allocation

Clearly, the DBS's location and the resource allocation policy are mutually dependent. We decompose this joint optimization problem into two subproblems including the 3D DBS placement problem and the resource allocation problem. We try to solve the resource allocation problem first and then utilize its optimal solutions to address the 3D DBS placement problem. We next discuss these two subproblems in detail.

### 3.3.1   Resource Allocation Problem

In the resource allocation problem, bandwidth and power are allocated to the users to maximize the total data rate with consideration of QoS requirement and resource limitation. The resource allocation problem can be formulated as

$$\textbf{P1:} \max_{\beta_i, P_i} \sum_{i=1}^{|\mathcal{I}|} R_i \tag{3.20}$$

$$s.t. \quad (3.11), (3.12), (3.13), (3.14), (3.18), (3.19).$$

In **P1**, Constraint (3.12) can be omitted as the capacity of FSO is assumed high enough which can reach 10 Gbps at the range of 1 km under clear weather condition

[5]. Furthermore, the equality condition in Constraints (3.13) and (3.14) should always hold to maximize the objective function (3.20) because given an allocation policy of $\beta_i$ and $P_i$ which are less than the maximal bandwidth and power allowed, we can always find a higher value of each $\beta_i$ and $P_i$ that increase the value of the objective function. Hence, the optimal value of the objective function is reached when the equality condition of (3.13) and (3.14) hold. Then, problem **P1** can be transformed into

$$\textbf{P1-a}: \max_{\beta_i, P_i} \sum_{i=1}^{|\mathcal{I}|} R_i$$

$$s.t. \quad (3.11), (3.18), (3.19),$$

$$\sum_{i=1}^{|\mathcal{I}|} \beta_i = B, \tag{3.21}$$

$$\sum_{i=1}^{|\mathcal{I}|} P_i = P_{max}, \tag{3.22}$$

**Lemma 2.** *P1-a is a concave optimization problem.*

*Proof.* In **P1-a**, we can see that Constraints (3.18), (3.19), (3.21) and (3.22) are all linear functions. Thus, if $R_i$ can be proven to be a concave function of $\beta_i$ and $P_i$, then **P1-a** is a concave optimization problem (note that the objective function is also concave because a sum of concave functions is also concave). Next, we try to prove the convexity of $R_i$. To show that $R_i$ is concave in $(\beta_i, P_i)$, we derive the Hessian matrix, which is

$$\nabla^2 R_i = \frac{-\alpha_i}{\beta_i(1 + \alpha_i P_i/\beta_i)^2} \begin{bmatrix} 1 \\ -P_i \end{bmatrix} \begin{bmatrix} 1 \\ -P_i \end{bmatrix}^{\mathrm{T}}, \tag{3.23}$$

**19**

where $\alpha_i = (10^{\frac{-\xi_i}{10}})/n_0$ and $[\cdot]^{\mathrm{T}}$ denotes the transpose operation. Since $\alpha_i$, $\beta_i$ and $P_i$ are positive, $\nabla^2 R_i$ is negative semidefinite, which implies that $R_i$ is a concave function of $\beta_i$ and $P_i$. $\qquad\qquad\square$

To solve **P1-a**, many off-the-shelf tools, such as CVX and CPLEX [36], can be utilized to acquire the optimal numerical solutions.

### 3.3.2 3D DBS Placement Problem

In the 3D DBS placement problem, given the resource allocation policy to the users, we determine the 3D location of the DBS while maximizing the throughput of the access link. Hence, the 3D DBS placement problem can be formulated as

$$\textbf{P2:} \max_{x,y,h} \sum_{i=1}^{|\mathcal{I}|} R_i$$

$$s.t. \quad (3.11), (3.25), (3.26), (3.27).$$

In problem **P2**, $\beta_i$ and $P_i$ are given, and $R_i$ is a function of $\xi_i$, i.e., $R_i = g(\xi_i)$. Thus, Constraint (3.11) $R_i \geq T_i$, i.e., $g(\xi_i) \geq T_i$, can be rewritten as $\xi_i \leq g^{-1}(T_i)$. Problem **P2** can be reformulated as

$$\textbf{P2-a:} \max_{x,y,h} \sum_{i=1}^{|\mathcal{I}|} R_i$$

$$s.t. \quad \xi_i \leq g^{-1}(T_i) \tag{3.24}$$

$$x^{min} \leq x \leq x^{max}, \tag{3.25}$$

$$y^{min} \leq y \leq y^{max}, \tag{3.26}$$

$$h^{min} \leq h \leq h^{max}, \tag{3.27}$$

Note that now the QoS requirement of users is denoted by pathloss which is given by Constraint (3.24). That is, violating the pathloss requirement is equivalent to not satisfying the data rate requirement. However, **P2-a** is still difficult to solve because Equation (3.1) is non-linear and non-convex with respect to $x$, $y$ and $h$. Thus, we design a heuristic algorithm to efficiently solve it.

The basic idea of the heuristic algorithm is to decompose the 3D DBS placement into the horizontal placement and vertical placement , respectively. First, we decide the vertical location of the DBS based on Definition 2. Second, we exhaustively search for all the candidate locations in the horizontal dimension that maximizes the aggregated data rate of all users. Specifically,

First, a given hotspot area is divided into a number of locations with the same size (e.g., $10 \ m \times 10 \ m$). Denote $\mathcal{K}$ as the set of these locations and $k$ is used to index these locations. Thus, DBS would be deployed over these locations.

Second, find user $\bar{i}$ that has the lowest pathloss requirement among the users in $\mathcal{I}$, i.e., $\bar{i} = \arg\min_{i} \{g^{-1}(T_i) \,|\, i \in \mathcal{I}\}$. The altitude of the DBS is set to be $h_{\bar{i}}^*$. Note that, based on Lemma 1, we can derive that the users within the user association area of the DBS can always meet their pathloss requirements (i.e., data rate requirements) if they are associated to the DBS. We iteratively place the DBS over different locations in the hotspot area with the altitude of $h_{\bar{i}}^*$. The DBS will be finally placed over the location $k^*$, which incurs the largest value of $\sum_{i=1}^{|\mathcal{I}|} R_i$ among other locations, i.e.,

$$k^* = \arg\max_{k} \left\{ \sum_{i=1}^{|\mathcal{I}|} R_i \,|\, k \in \mathcal{K} \right\}. \tag{3.28}$$

The algorithm is summarized in Algorithm 1. The complexity of Steps 3-4 is $O(|\mathcal{I}|)$; that of Steps 6-8 is $O(|\mathcal{I}||\mathcal{K}|)$; that of Steps 9 is also $O(|\mathcal{I}||\mathcal{K}|)$, and they can repeat for at most $O(|\mathcal{K}|)$ times. Therefore, the complexity of the CIDER algorithm is $O(|\mathcal{K}||\mathcal{I}|+|\mathcal{K}|^2|I|)$.

---
**Algorithm 1:** CIDER
---

**1** Initialize $x$, $y$, $h$, $\mathcal{K}$.

**2 while** $\sum\limits_{i=1}^{|\mathcal{I}|} R_i$ *increases* **do**

**3**     Obtain $\beta_i$ and $P_i$ by solving **P1-a**;

**4**     Find user $\bar{i}$, where $\bar{i} = \arg\min\limits_{i} \{g^{-1}(T_i) \,|\, i \in \mathcal{I}\}$;

**5**     Set $h = h_{\bar{i}}^*$;

**6**     **for** $k = 1$ *to* $|\mathcal{K}|$ **do**

**7**         Obtain $\sum\limits_{i=1}^{|\mathcal{I}|} R_i$ at location $k$;

**8**     **end**

**9**     Obtain location $k^*$ based on Equation (3.28);

**10**     Set $h = h_{\bar{i}}^*$ and update $x$ and $y$ based on $k^*$.

**11 end**
---

### 3.4   Simulations

In this section, simulation results are provided to validate the performance of CIDER. We consider a hotspot area located in an urban area. The size of the hotspot area is $500 \; m \times 500 \; m$. The locations of users in the hotspot area are generated based on the spatial Poisson point process. The size of each location $k$ in the hotspot area is $10 \; m \times 10 \; m$. The QoS requirements among the users are modeled based on the Poisson distribution with the average value of $50 \; Kbps$. Other simulation parameters are shown in Table 3.2. In the simulation results, we compare the performance of our proposed algorithm with the Stationary DBS placement and equal resource allocation approach. In the latter case, the DBS is assumed to be deployed at the center of the hotspot area with fixed altitude $h = 50 \; m$. At the same time, equal resources are allocated to all the users. We also compare our proposed approach with the traditional scheme (denoted by 'No FSO' in the figures) where separate frequency spectra are

employed in the backhaul link. In this scheme, half of the total available bandwidth is dedicated to the backhaul link, while the other half is equally allocated to the users. The location of the DBS in this approach is the same as in the first benchmark approach.

**Table 3.2** Simulation Parameters I

| Parameters | Definition | Value |
|---|---|---|
| $a$ | Environment parameter | 9.61 |
| $b$ | Environment parameter | 0.16 |
| $\eta_{LoS}$ | Average excessive pathloss of having an LoS | $1\ dB$ |
| $\eta_{NLoS}$ | Average excessive pathloss of having an NLoS | $20\ dB$ |
| $f$ | Carrier frequency | $2\ GHz$ |
| $n_0$ | Noise power spectral density | $140\ dBm$ |
| $B$ | Total available bandwidth | $20\ MHz$ |
| $P_{max}$ | Total available power | $0.5\ mW$ |

Figure 3.3 shows a snapshot of the users' locations which are generated based on a spatial Poisson point process as well as the DBS's 3D location incurred by CIDER. In this figure, the DBS is deployed to serve 500 users in the hotspot area. The QoS requirements of all users are met by leveraging the DBS. The 3D location of the DBS and the resource allocation policy are determined based on the locations of the users and their corresponding QoS requirements.

Figure 3.4 shows the total throughput of the access link for satisfied QoS requirement versus the number of users in the hotspot area. From Figure 3.4, we can see the throughput of our proposed approach is nearly twice that of the stationary DBS and equal resource allocation approach. Furthermore, the throughput of our proposed approach decreases because as the number of users increases, less
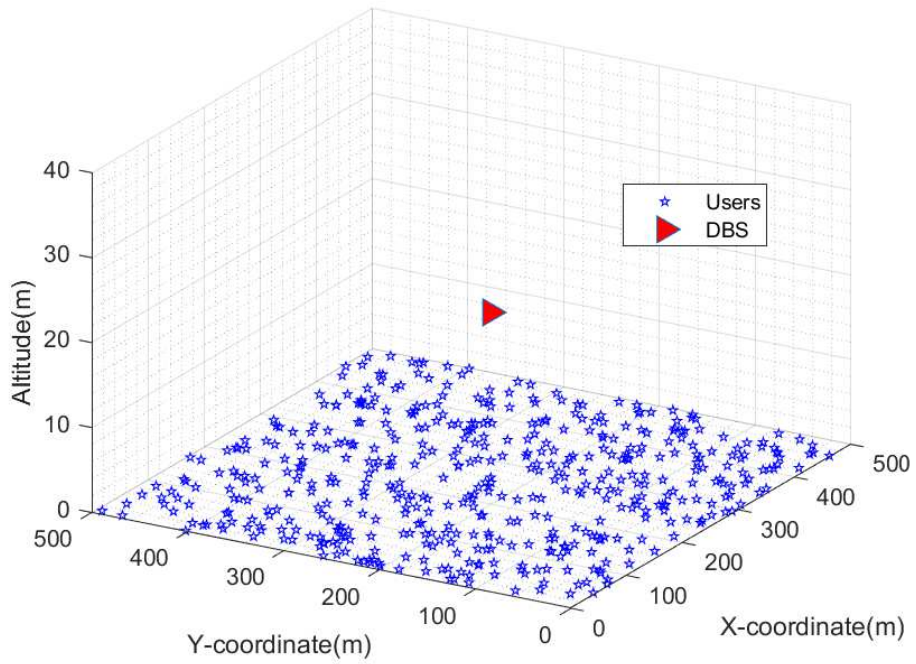
**Figure 3.3** Snapshot of DBS's and users' locations incurred by DIDER.
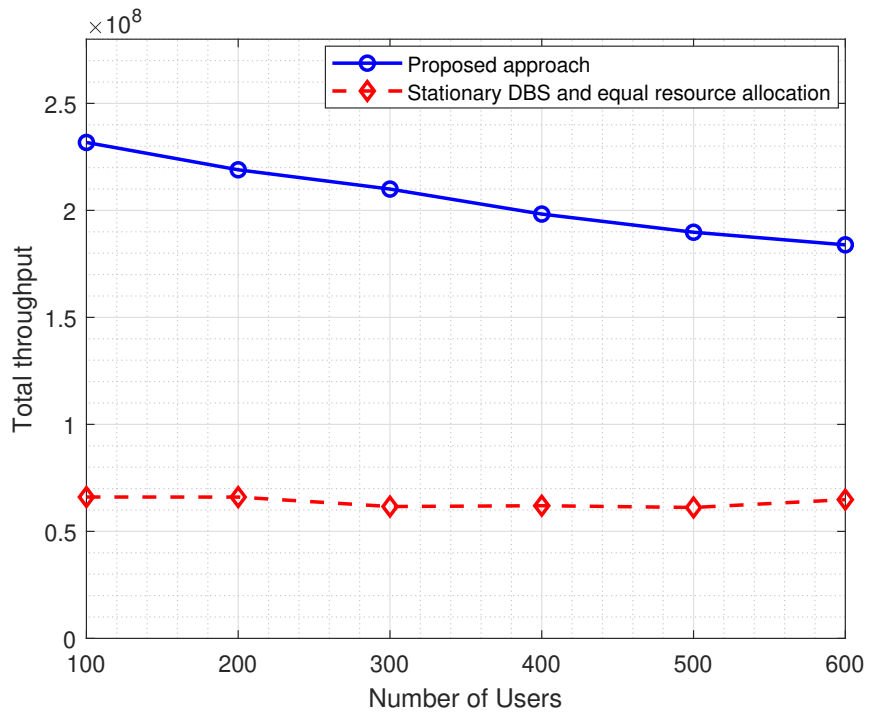


**Figure 3.4** Throughput versus number of users.
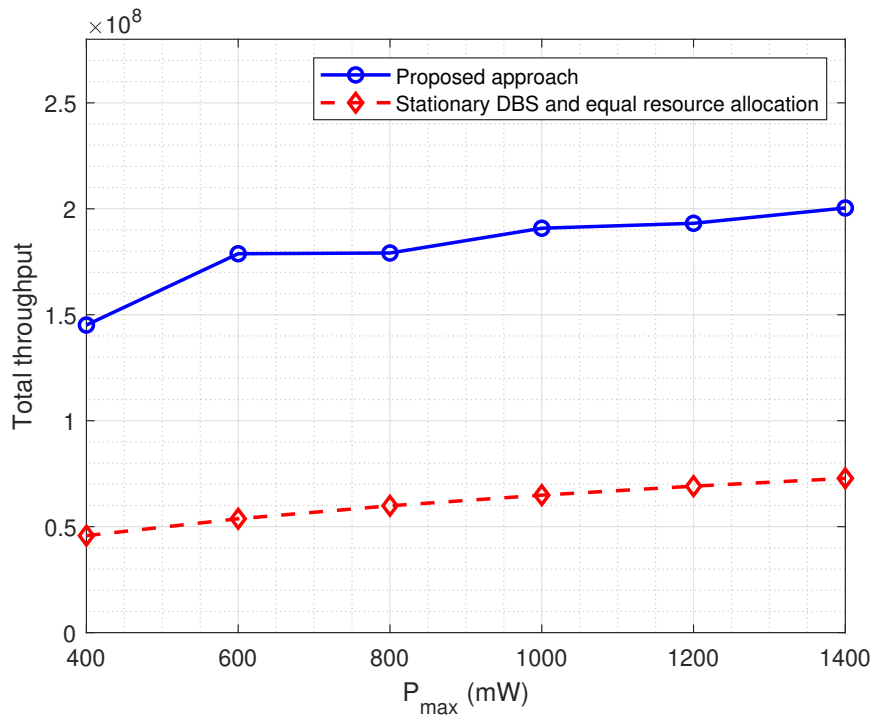
**Figure 3.5** Throughput versus total available power.
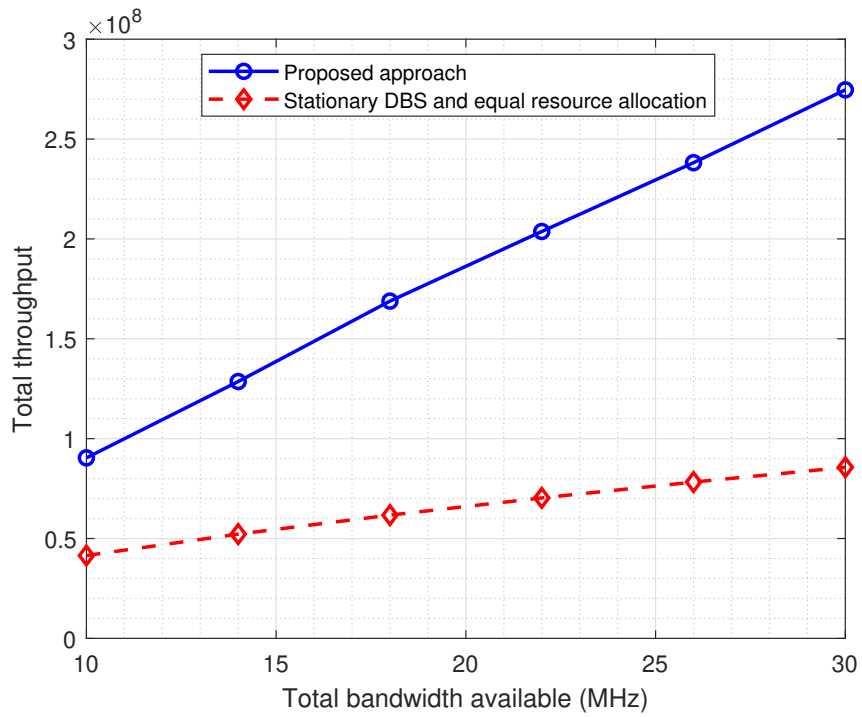


**Figure 3.6** Throughput versus total available bandwidth.

resources are leftover to be allocated to maximize the throughput. The throughput of the benchmark algorithms stay roughly constant because the users are uniformly distributed across the whole area and equal resource is allocated to all of them.

Figures 3.5 and 3.6 illustrate how the total available resource of the DBS affects the total throughput. We can see that the total throughput increases as the total available resource increases in both cases. Our proposed approach achieves higher throughput as compared to the benchmark algorithms because the throughput can be improved by allocating more resource to the users with lower pathloss, and it can also be improved by moving to the positions which incur lower pathloss based on our proposed algorithm.

# CHAPTER 4

# LATENCY MINIMIZATION

In this chapter, we propose to deploy a DBS to serve the ground users by offloading their traffic from the MBS to the DBS. The FSO technique is employed to avoid interference with the access link and provide a high-capacity backhaul link. A latency ratio minimization problem is formulated to optimize the DBS's location, user association and bandwidth allocation subject to user QoS requirements and limited available bandwidth constraints.

## 4.1 System Model and Problem Formulation

As shown in Figure 4.1, the latency of users can be reduced by offloading traffic from the MBS to the DBS since a better channel condition can be provisioned. The FSO link is working as the backhaul due to it high potential capacity. We assume that the Frequency Division Multiple Access (FDMA) mode is adopted in the access link to avoid interference among users.

### 4.1.1 Traffic Load Model of the MBS

We assume that the traffic of user $i$ is generated according to a Poisson process with the arrival rate $\lambda_i$. The traffic sizes of all requests follow a general distribution with the average value of $v_i$. Therefore, the average traffic load of user $i$ can be obtained as $\lambda_i v_i$.

The data rate of user $i$ which is associated with the MBS, denoted as $r_i^M$, can be expressed as

$$r_i^M = \beta^M \log_2(1 + \frac{P^M 10^{-\frac{\eta_i^M}{10}}}{\sigma^2})$$

(4.1)
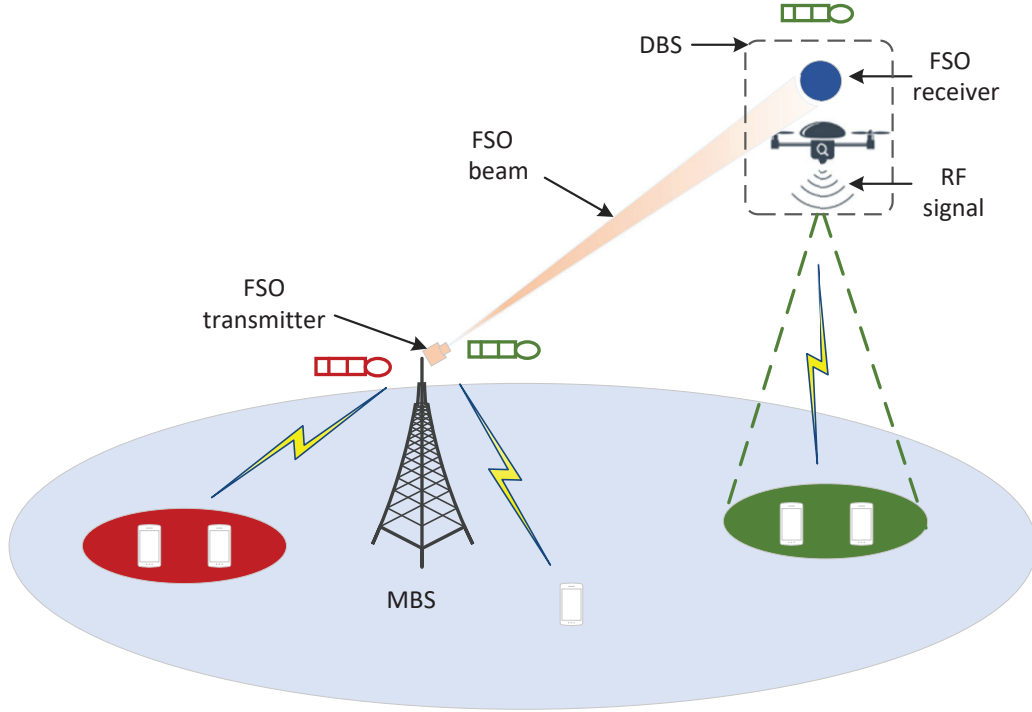
**Figure 4.1** Probabilistic pathloss model.

where $P^M$ is the transmit power of the MBS, $\beta^M$ is the amount of bandwidth allocated to the MBS, $\sigma^2$ is the environment noise power, and $\eta_i^M$ is the pathloss between user $i$ and the MBS, which can be modeled as

$$\eta_i^M = \alpha + \gamma \log_{10}(d_i^M). \tag{4.2}$$

Here, $\alpha$ is the path loss at the reference distance and $\gamma$ is the path loss exponent, and $d_i^M$ is the distance between the MBS and user $i$, i.e.,

$$d_i^M = \sqrt{(x_i - x^M)^2 + (y_i - y^M)^2}, \tag{4.3}$$

where $(x_i, y_i)$ and $(x^M, y^M)$ are the locations of user $i$ and the MBS, respectively. The average utilization of the MBS that indicates the fraction of time during which the MBS is busy serving user $i$ can be calculated as

$$\rho_i^M = \frac{\lambda_i v_i}{r_i^M}. \tag{4.4}$$

Thus, by summing up the traffic of all users associated with the MBS, the average utilization of the MBS can be calculated as

$$\rho^M = \sum_{i=1}^{|\mathcal{I}|} \rho_i^M (1 - \theta_i) = \frac{\lambda_i v_i (1 - \theta_i)}{r_i^M}, \tag{4.5}$$

where $\theta_i$ is the binary variable to indicate whether user $i$ is associated with the DBS (i.e., $\theta_i = 1$) or not (i.e., $\theta_i = 0$).

Assume that the traffic arrival of users associated with the MBS are independent. The arrival stream, which is formed by merging all the traffic from users associated with the MBS, is also a Poisson process (recall that the traffic arrival of each user is a Poisson process). Thus, user $i$'s (associated with the MBS) service time can be obtained as $s_i^M = v_i / r_i^M$. In addition, the traffic size $v_i$ follows a general distribution such that the service time of user $i$ also satisfies a general distribution. Therefore, based on queuing theory, the MBS's downlink transmission process realizes an M/G/1 processor sharing queue. For user $i$ which is associated with the MBS, the corresponding average traffic delivery time, including the waiting time and service time, is [37, 38]

$$T_i^M = \frac{s_i^M}{1 - \rho^M}. \tag{4.6}$$

Based on the average traffic delivery time, the average traffic latency ratio $\tau_i^M$ can be calculated as

$$\tau_i^M = \frac{T_i^M - s_i^M}{s_i^M} = \frac{\rho^M}{1 - \rho^M}, \tag{4.7}$$

where the value of $\tau_i^M$ implies the waiting time of user $i$ to receive a unit service time. From Equation (4.7), we can observe that $\tau_i^M$ is independent of user index $i$, which

indicates that the average latency ratio of users associated with the MBS share the same value, i.e.,

$$\tau^M = \frac{\rho^M}{1 - \rho^M}. \tag{4.8}$$

### 4.1.2 Traffic Load Model of the DBS

Note that a two-hop communication is incurred when users are associated with the DBS. Therefore, two queues are generated in the access link (the link between a user and the DBS) and the backhaul link (the link between the DBS and the MBS), respectively. Following the similar derivation process, the average latency ratio of users associated with the DBS in the access link can be obtained as

$$\tau^{D,a} = \frac{\rho^{D,a}}{1 - \rho^{D,a}}, \tag{4.9}$$

where $\rho^{D,a}$ is the average utilization of users (associated with the DBS) in the access link, i.e.,

$$\rho^{D,a} = \sum_{i=1}^{|\mathcal{I}|} \rho_i^{D,a} \theta_i = \frac{\lambda_i v_i \theta_i}{r_i^{D,a}}, \tag{4.10}$$

where $r_i^{D,a}$ is user $i$'s data rate of the access link. Thus, we have

$$r_i^{D,a} = \beta^M \log_2(1 + \frac{P^D 10^{-\frac{\eta_i^D}{10}}}{\sigma^2}), \tag{4.11}$$

where $P^D$ is the transmit power of the DBS, $\beta^D$ is the amount of bandwidth allocated to the DBS and $\eta_i^D$ is the pathloss between the DBS and user $i$.

Similarly, the average latency ratio in the backhaul link can be obtained as

$$\tau^{D,b} = \frac{\rho^{D,b}}{1 - \rho^{D,b}}, \tag{4.12}$$

where $\rho^{D,b}$ is the average utilization of the backhaul link, i.e.,

$$\rho^{D,b} = \sum_{i=1}^{|\mathcal{I}|} \rho_i^{D,b} \theta_i = \frac{\lambda_i v_i \theta_i}{r_i^{D,b}}, \tag{4.13}$$

where $r_i^{D,b}$ is user $i$'s data rate of the FSO-based backhaul link, which can be obtained as [5]

$$r_i^{D,b} = \frac{P_t \eta_t \eta_r 10^{-\frac{L_{atm}}{10}} 10^{-\frac{L_{geo}}{10}}}{E_p N_b}, \tag{4.14}$$

where $P_t$ is the transmission power of the laser, and $\eta_t$ and $\eta_r$ denote the transmitting efficiency and receiving efficiency, respectively. $E_p = h_p c / \lambda_c$ is the photon energy. $\lambda_c$ is the carrier wavelength, $h_p$ denotes Plank's constant. $N_b$ implicates the receiver sensitivity (photons/bit). $L_{geo} = 10 \log(\frac{\pi r^2}{\pi(\psi_t l/2)^2})$ is the geometrical loss in dB, $l$ is the distance between the laser transmitter and receiver in Km, $r$ is the radius of the receiver's aperture in m, and $\psi_t$ denotes the transmitting divergence angle. $L_{atm} = \frac{17}{V}(\frac{\lambda}{550nm})^{-q}$ stands for the atmospheric attenuation caused by bad weather conditions, where $L_{atm}$ is in dB/Km, $q$ is the size distribution of the scattering particles under different weather conditions, $V$ is the visibility in Km. The value of $q$ is determined by Equation (3.9).

## 4.2   Problem Formulation

As mentioned previously, the deployment of the DBS reduces users' latency by enabling the traffic offloaded from the MBS to the DBS since a better channel condition is provided. Our goal is to minimize the overall latency ratio of users while considering the QoS requirements of users and the limited available resource. Specifically,

$$\textbf{P0:} \min_{x,y,h,\theta_i,\beta^M,\beta^D} \sum_{i=1}^{|\mathcal{I}|} \tau^{D,a} + \tau^{D,b} + \tau^M \tag{4.15}$$

$$s.t. \quad r_i^{D,a}\theta_i + r_i^M(1-\theta_i) \geq T_i, \forall i \in \mathcal{I}, \tag{4.16}$$

$$\tau^{D,a} + \tau^{D,b} \leq \epsilon, \forall i \in \mathcal{I}, \tag{4.17}$$

$$\tau^M \leq \epsilon, \forall i \in \mathcal{I}, \tag{4.18}$$

$$\beta^M + \beta^D = B, \tag{4.19}$$

$$\beta^M, \beta^M \geq 0, \tag{4.20}$$

$$\theta_i \in \{0,1\}, \forall i \in \mathcal{I}, \tag{4.21}$$

$$0 \leq \rho^{D,a}, \rho^{D,b}, \rho^M < 1, \tag{4.22}$$

where $T_i$ indicates user $i$'s data rate requirement, and $x$, $y$, and $h$ are the 3D location of the DBS. $\epsilon$ denotes the latency ratio requirement. $B$ is the total available bandwidth. Constraints (4.16), (4.17) and (4.18) enforce the QoS and latency requirement of each user. Constraint (4.19) stands for the resource limitations. Constraint (4.20) imposes the bandwidth allocated to the MBS and DBS to be non-negative. Constraint (4.21) imposes $\theta_i$ to be a binary variable. Constraint (4.22) ensures the stability of the queuing system.

Since the latency ratio is a monotonically increasing function of utilization if $0 \leq \rho < 1$ (remember $\tau = \frac{\rho}{1-\rho}$), we can minimize the latency ratio by minimizing the utilization. Meanwhile, we omit the latency ratio incurred in the backhaul link since the capacity of FSO is sufficiently high. According to [5, 25], the data rate of a FSO link can reach 10 Gbps under clear weather condition within the range of 1 Km. Therefore, **P0** can be transformed into the following problem **P0-a**

$$\textbf{P0-a:} \min_{x,y,h,\theta_i,\beta^M,\beta^D} \quad \rho^{D,a} + \rho^M$$

$$s.t. \quad \tau^{D,a} \leq \epsilon, \forall i \in \mathcal{I}, \tag{4.23}$$

$$(4.16),(4.18),(4.19),(4.20),(4.21),(4.22).$$

Unfortunately, **P0-a** is a mixed integer non-linear non-convex problem and thus challenging to solve considering Equation (3.2) and Constraint (4.16). Next, we propose an efficient framework to solve this optimization problem. In essence, we partition the entire decision variables into two blocks. In each iteration, the bandwidth allocation and user association policy, and the location of the DBS are alternately optimized, i.e., one block is optimized at each iteration while keeping the other block fixed. We iteratively optimize these two blocks until the user association, DBS's location and bandwidth allocation are determined.

## 4.3 DBS Placement, Bandwidth Allocation and User Association

To make **P0-a** more tractable, we decompose this joint optimization problem into two subproblems, i.e., the bandwidth allocation and user association problem and the DBS placement problem.

### 4.3.1 Bandwidth Allocation and User Association

In this subproblem, for any fixed location of the DBS, we determine the amount of bandwidth allocated to the MBS and DBS and whether each user should be associated with the MBS or DBS to minimize the overall latency ratio. The bandwidth allocation and user association problem can be formulated as

$$\textbf{P1:} \min_{\theta_i, \beta^M, \beta^D} \sum_{i=1}^{|\mathcal{I}|} \frac{\lambda_i v_i \theta_i}{r_i^{D,a}} + \sum_{i=1}^{|\mathcal{I}|} \frac{\lambda_i v_i (1 - \theta_i)}{r_i^M} \qquad (4.24)$$

$$s.t. \quad (4.16), (4.18), (4.19), (4.20), (4.21), (4.22), (4.23).$$

Since $\tau = \frac{\rho}{1-\rho} \leq \epsilon$ is equivalent to $\rho \leq \frac{\epsilon}{1+\epsilon}$, Constraint (4.22) is always satisfied if Constraints (4.23) and (4.18) are satisfied. Problem **P1** can be simplified by removing Constraint (4.22). The problem is still challenging due to the non-continuity of $\theta_i$. We relax $\theta_i$ as a continuous variable (i.e., $0 \leq \theta_i \leq 1, \forall i \in \mathcal{I}$). Finally, Problem **P1** can be rewritten as

$$\textbf{P1-a:} \min_{\theta_i, \beta^M, \beta^D} \sum_{i=1}^{|\mathcal{I}|} \frac{\lambda_i v_i \theta_i}{\beta^D \iota_i} + \sum_{i=1}^{|\mathcal{I}|} \frac{\lambda_i v_i (1 - \theta_i)}{\beta^M \kappa_i} \qquad (4.25)$$

$$s.t. \quad \beta^M \kappa_i \theta_i - \beta^D \iota_i \theta_i - \beta^M \kappa_i + T_i \leq 0, \qquad (4.26)$$

$$\sum_{i=1}^{|\mathcal{I}|} \frac{\lambda_i v_i}{\iota_i} \theta_i - \frac{\epsilon}{\epsilon + 1} \beta^D \leq 0, \qquad (4.27)$$

$$\sum_{i=1}^{|\mathcal{I}|} \frac{\lambda_i v_i}{\kappa_i} (1 - \theta_i) - \frac{\epsilon}{\epsilon + 1} \beta^M \leq 0, \qquad (4.28)$$

$$0 \leq \theta_i \leq 1, \forall i \in \mathcal{I}, \qquad (4.29)$$

$$(4.19), (4.20),$$

where $\iota_i = \log_2(1 + \frac{P^D 10^{-\frac{\eta_i^D}{10}}}{\sigma^2})$ and $\kappa_i = \log_2(1 + \frac{P^M 10^{-\frac{\eta_i^M}{10}}}{\sigma^2})$. We can see that all the constraints are linear except Constraint (4.26). If we can prove that Constraint (4.26) is a convex set, P1-a is a sum-of-ratios problem [39, 40] since the numerators are all convex and the denominators are all concave (note that a linear function is both convex and concave).

Next, we prove that Constraint (4.26) is a convex funciton. Since $-\beta^M \kappa_i + T_i$ is linear, it will not affect the convexity of Constraint (4.26). Thus, proving Constraint (4.26) is convex is equivalent to proving $\beta^M \kappa_i \theta_i - \beta^D \iota_i \theta_i$ is convex. Its Hessian matrix

w.r.t. $\beta^D$, $\beta^M$ and $\theta_i$ can be derived as

$$H = \begin{bmatrix} 0 & 0 & -\iota_i \\ 0 & 0 & \kappa_i \\ -\iota_i & \kappa_i & 0 \end{bmatrix}. \tag{4.30}$$

Since $\iota_i$, $\kappa_i$ are all positive, it can be easily proved that $H$ is positive semi-definite; so Constraint (4.26) is a convex set, and P1-a is a sums-of-ratios problem [39] which can be resolved by applying algorithm proposed in [41]. It is easy to see that **P1-a** is equivalent to the following problem

$$\textbf{P1-b:} \min_{\theta_i, \omega_i, \beta^M, \beta^D} \sum_{i=1}^{2|\mathcal{I}|} \omega_i \tag{4.31}$$

$$s.t. \quad \frac{\lambda_i v_i \theta_i}{\beta^D \iota_i} \leq \omega_i, \ 1 \leq i \leq |\mathcal{I}| \tag{4.32}$$

$$\frac{\lambda_i v_i (1 - \theta_i)}{\beta^M \kappa_i} \leq \omega_{i+|\mathcal{I}|}, 1 \leq i \leq |\mathcal{I}| \tag{4.33}$$

$$(4.19), (4.20), (4.26), (4.27), (4.28), (4.29),$$

where $\omega_i$ is the introduced relaxation variable. Then, the Lagrangian function of **P1-b** is

$$\mathcal{L}(\boldsymbol{\theta}, \boldsymbol{\beta}, \boldsymbol{\omega}, \boldsymbol{\mu}, \boldsymbol{\varrho}) = \sum_{i=1}^{2|\mathcal{I}|} \omega_i + \sum_{i=1}^{|\mathcal{I}|} \mu_i (\lambda_i v_i \theta_i - \omega_i \beta^D \iota_i)$$

$$+ \sum_{i=1}^{|\mathcal{I}|} \mu_{i+|\mathcal{I}|} [\lambda_i v_i (1 - \theta_i) - \omega_{i+|\mathcal{I}|} \beta^M \kappa_i]$$

$$+ \sum_{i=1}^{|\mathcal{I}|} \varrho_{i+2|\mathcal{I}|} (\beta^M \kappa_i \theta_i - \beta^D \iota_i \theta_i - \beta^M \kappa_i + T_i)$$

$$+ \varrho_{3|\mathcal{I}|+1} \left( \sum_{i=1}^{|\mathcal{I}|} \frac{\lambda_i v_i}{\iota_i} \theta_i - \frac{\epsilon}{\epsilon + 1} \beta^D \right)$$

$$+ \varrho_{3|\mathcal{I}|+2} \left[ \sum_{i=1}^{|\mathcal{I}|} \frac{\lambda_i v_i}{\kappa_i} (1 - \theta_i) - \frac{\epsilon}{\epsilon + 1} \beta^M \right]$$

$$+ \varrho_{3|\mathcal{I}|+3} (\beta^M + \beta^D - B)$$

$$+ \sum_{i=1}^{|\mathcal{I}|} \varrho_i (-\theta_i) + \sum_{i=1}^{|\mathcal{I}|} \varrho_{i+|\mathcal{I}|} (\theta_i - 1) \tag{4.34}$$

where $\boldsymbol{\mu}$ and $\boldsymbol{\varrho}$ are the Lagrangian multipliers of the constraints.

The Karush-Kuhn-Tucker (KKT) conditions are

$$\frac{\partial \mathcal{L}}{\theta_i} = \mu_i \lambda_i v_i - \mu_{i+|\mathcal{I}|} \lambda_i v_i + \varrho_{i+2|\mathcal{I}|} (\beta^M \kappa_i - \beta^D \iota_i)$$

$$+ \varrho_{3|\mathcal{I}|+1} \frac{\lambda_i v_i}{\iota_i} - \varrho_{3|\mathcal{I}|+2} \frac{\lambda_i v_i}{\kappa_i} - \varrho_i + \varrho_{i+|\mathcal{I}|} = 0, \tag{4.35}$$

$$\frac{\partial \mathcal{L}}{\beta^D} = \sum_{i=1}^{|\mathcal{I}|} -\mu_i \omega_i \iota_i - \sum_{i=1}^{|\mathcal{I}|} \varrho_{i+2|\mathcal{I}|} \iota_i \theta_i$$

$$- \varrho_{3|\mathcal{I}|+1} \frac{\epsilon}{\epsilon + 1} + \varrho_{3|\mathcal{I}|+3} = 0, \tag{4.36}$$

$$\frac{\partial \mathcal{L}}{\beta^M} = \sum_{i=1}^{|\mathcal{I}|} -\mu_{i+|\mathcal{I}|}\omega_{i+|\mathcal{I}|}\kappa_i - \sum_{i=1}^{|\mathcal{I}|} \varrho_{i+2|\mathcal{I}|}(\kappa_i\theta_i - \kappa_i)$$

$$- \varrho_{3|\mathcal{I}|+2}\frac{\epsilon}{\epsilon+1} + \varrho_{3|\mathcal{I}|+3} = 0, \tag{4.37}$$

$$\frac{\partial \mathcal{L}}{\omega_i} = \begin{cases} 1 - \mu_i\beta^D\iota_i, & 1 \le i \le |\mathcal{I}|, \\ 1 - \mu_i\beta^M\kappa_{i-|\mathcal{I}|}, & |I|+1 \le i \le 2|I|, \end{cases}$$

$$= 0, \tag{4.38}$$

$$\mu_{i+|\mathcal{I}|}[\lambda_i v_i(1-\theta_i) - \omega_{i+|\mathcal{I}|}\beta^M\kappa_i] = 0,$$

$$\mu_i(\lambda_i v_i\theta_i - \omega_i\beta^D\iota_i) = 0, 1 \le i \le |\mathcal{I}|, \tag{4.39}$$

$$\varrho_i(-\theta_i) = 0, \varrho_{i+|\mathcal{I}|}(\theta_i - 1) = 0, \tag{4.40}$$

$$\varrho_{i+2|\mathcal{I}|}(\beta^M\kappa_i\theta_i - \beta^D\iota_i\theta_i - \beta^M\kappa_i + T_i) = 0, \tag{4.41}$$

$$\varrho_{3|\mathcal{I}|+1}\left(\sum_{i=1}^{|\mathcal{I}|} \frac{\lambda_i v_i}{\iota_i}\theta_i - \frac{\epsilon}{\epsilon+1}\beta^D\right) = 0, \tag{4.42}$$

$$\varrho_{3|\mathcal{I}|+2}\left[\sum_{i=1}^{|\mathcal{I}|} \frac{\lambda_i v_i}{\kappa_i}(1-\theta_i) - \frac{\epsilon}{\epsilon+1}\beta^M\right] = 0, \tag{4.43}$$

$$\varrho_{3|\mathcal{I}|+3}(\beta^M + \beta^D - B) = 0, \tag{4.44}$$

$$(4.19), (4.20), (4.26) - (4.29).$$

Equation (4.38) is equivalent to

$$\begin{cases} \mu_i = \frac{1}{\beta^D \iota_i}, & 1 \le i \le |\mathcal{I}|, \\ \mu_{i+|\mathcal{I}|} = \frac{1}{\beta^M \kappa_i}, & 1 \le i \le |\mathcal{I}|, \end{cases} \tag{4.45}$$

which is substituted into Equation (4.39) to yield

$$\begin{cases} \lambda_i v_i(1 - \theta_i) - \omega_{i+|\mathcal{I}|}\beta^M \kappa_i = 0, & 1 \le i \le |\mathcal{I}|, \\ \lambda_i v_i \theta_i - \omega_i \beta^D \iota_i = 0, & 1 \le i \le |\mathcal{I}|. \end{cases} \quad (4.46)$$

Note that Equations(4.35)-(4.37), Equations (4.40)-(4.44) and Equations (4.26)-(4.29) are KKT conditions of problem **P2** if $\omega_i$ and $\mu_i$ are fixed.

$$\mathbf{P2:} \min_{\theta_i, \beta^M, \beta^D} \sum_{i=1}^{|\mathcal{I}|} \mu_i(\lambda_i v_i \theta_i - \omega_i \beta^D \iota_i)$$

$$+ \sum_{i=1}^{|\mathcal{I}|} \mu_{i+|\mathcal{I}|}[\lambda_i v_i(1 - \theta_i) - \omega_{i+|\mathcal{I}|}\beta^M \kappa_i]$$

$$s.t. \quad (4.19), (4.20), (4.26) - (4.29). \quad (4.47)$$

For fixed $\boldsymbol{\mu}$ and $\boldsymbol{\varrho}$, the objective function of **P2** is convex and thus **P2** is a convex optimization problem. Therefore, we conclude that the solution of problem **P2** can be obtained by finding those satisfying Equations (4.45) and (4.46) among the solutions of the convex problem **P2**.

Denote $\boldsymbol{x} = [\boldsymbol{\omega}; \boldsymbol{\mu}]$ and $\theta_i(x)$, $\beta^D(x)$ and $\beta^M(x)$ as the solution of problem **P2**. To satisfy Equations (4.45) and (4.46), we have $(1 \le i \le |\mathcal{I}|)$

$$\begin{cases} \mu_i \beta^D \iota_i - 1 = 0, \\ \mu_{i+|\mathcal{I}|}\beta^M \kappa_i - 1 = 0, \\ \omega_i \beta^D \iota_i - \lambda_i v_i \theta_i = 0, \\ \omega_{i+|\mathcal{I}|}\beta^M \kappa_i - \lambda_i v_i(1 - \theta_i) = 0. \end{cases} \quad (4.48)$$

Let $\phi_i(x) = \mu_i \beta^D \iota_i - 1$, $\phi_{i+|\mathcal{I}|}(x) = \mu_{i+|\mathcal{I}|}\beta^M \kappa_i - 1$, $\phi_{i+2|\mathcal{I}|}(x) = \omega_i \beta^D \iota_i - \lambda_i v_i \theta_i$ and $\phi_{i+3|\mathcal{I}|}(x) = \omega_{i+|\mathcal{I}|}\beta^M \kappa_i - \lambda_i v_i(1 - \theta_i)$. Thus, we have

$$\phi(\boldsymbol{x}) = [\phi_1(\boldsymbol{x}), ..., \phi_{|\mathcal{I}|}(\boldsymbol{x}), ..., \phi_{2|\mathcal{I}|}(\boldsymbol{x}),$$

$$..., \phi_{3|\mathcal{I}|}(\boldsymbol{x}), ..., \phi_{4|\mathcal{I}|}(\boldsymbol{x})]$$

$$= 0. \tag{4.49}$$

Thus, the solution of **P1-b** can be obtained by finding those satisfying (4.49) among the solutions of **P2**.

**Lemma 3.** $\phi(\boldsymbol{x})$ *is strongly monotone.*

*Proof: Let $f_i(x) = \beta^D \iota_i > 0$ and $f_{i+|\mathcal{I}|}(x) = \beta^M \kappa_i > 0$ for simplicity. The Jacobian matrix of $\phi(\boldsymbol{x})$ can be derived based on Equations (4.48) and (4.49) as*

$$\phi'(\boldsymbol{x}) = \begin{bmatrix} f_1(\boldsymbol{x}) & \cdots & 0 & 0 & \cdots & 0 \\ \vdots & \ddots & \vdots & \vdots & \ddots & \vdots \\ 0 & \cdots & f_{2|\mathcal{I}|}(\boldsymbol{x}) & 0 & \cdots & 0 \\ 0 & \cdots & 0 & f_1(\boldsymbol{x}) & \cdots & 0 \\ \vdots & \ddots & \vdots & \vdots & \ddots & \vdots \\ 0 & \cdots & 0 & 0 & \cdots & f_{2|\mathcal{I}|}(\boldsymbol{x}) \end{bmatrix}$$

*We can observe that $\phi'(\boldsymbol{x})$ is a positive definite matrix because $f_i(\boldsymbol{x}) > 0$, $(1 \leq i \leq 2|\mathcal{I}|)$. Therefore, $\phi(\boldsymbol{x})$ is strongly monotone.*

The modified Newton method [42] can be used to obtain the solution of (4.49). In each iteration, we update $\boldsymbol{x}$ by calculating

$$\boldsymbol{x}_{m+1} = \boldsymbol{x}_m + \delta_m \zeta_m, \tag{4.50}$$

where $m$ denotes the iteratioin number, and $\zeta_m$ denotes the search direction defined as

$$\zeta_m = -[\phi'(x)]^{-1}\phi(x)$$

$$= -\begin{bmatrix} \frac{1}{f_1(x)} & \cdots & 0 & 0 & \cdots & 0 \\ \vdots & \ddots & \vdots & \vdots & \ddots & \vdots \\ 0 & \cdots & \frac{1}{f_{2|\mathcal{I}|}(x)} & 0 & \cdots & 0 \\ 0 & \cdots & 0 & \frac{1}{f_1(x)} & \cdots & 0 \\ \vdots & \ddots & \vdots & \vdots & \ddots & \vdots \\ 0 & \cdots & 0 & 0 & \cdots & \frac{1}{f_{2|\mathcal{I}|}(x)} \end{bmatrix} \begin{bmatrix} \phi_1(x) \\ \vdots \\ \\ \vdots \\ \phi_{4|\mathcal{I}|}(x) \end{bmatrix}$$

$$= -\begin{bmatrix} \frac{\phi_1(x)}{f_1(x)} & \cdots & \frac{\phi_{2|\mathcal{I}|}(x)}{f_{2|\mathcal{I}|}(x)} & \frac{\phi_{2|\mathcal{I}|+1}(x)}{f_1(x)} & \cdots & \frac{\phi_{4|\mathcal{I}|}(x)}{f_{2|\mathcal{I}|}(x)} \end{bmatrix}^T$$

where $[.]^T$ denotes the transpose operation and $\delta_m \in (0,1)$ is the step length.

### 4.3.2   3D DBS Placement

For fixed bandwidth allocation and user association, we optimize the 3D location of the DBS aiming to minimize the overall latency ratio, i.e.,

$$\textbf{P3: } \min_{x,y,h} \quad \frac{1}{\beta^D}\sum_{i=1}^{|\mathcal{I}_1|}\frac{\lambda_i v_i}{\iota_i} \tag{4.51}$$

$$s.t. \quad \beta^D \iota_i \geq T_i, \forall i \in \mathcal{I}_1 \tag{4.52}$$

$$\sum_{i=1}^{|\mathcal{I}_1|}\frac{\lambda_i v_i}{\iota_i} \leq \frac{\epsilon}{\epsilon+1}\beta^D, \tag{4.53}$$

where $\mathcal{I}_1$ is the set of users associated with the DBS. Note that the second part of the objective function is omitted (which is incurred by users associated with the MBS) since it will stay fixed once the bandwidth allocation and user association are given. As $\beta^D$ and $T_i$ are known in **P3**, Constraint (4.52) can be rewritten as

$$\eta_i^D \leq -10\lg[(2^{\frac{T_i}{\beta^D}-1}-1)\frac{\sigma^2}{P^D}]. \tag{4.54}$$

Now the user data rate requirement is dictated by pathloss which is given by the above equation. Therefore, violating the pathloss requirement is equivalent to violating Constraint (4.52). We can further see that the minimal value of the objective function in **P3** should satisfy Constraint (4.53); otherwise, there would be no feasible solution for problem **P3**. Based on the above observations, we design an efficient heuristic algorithm to solve problem **P3**.

To make problem **P3** more tractable, we try to partition the decision variables of the 3D DBS location into two blocks (i.e., the horizontal location and vertical location) and solve them separately. In the vertical dimension, the flying height of the DBS is determined based on Definition 2. In the horizontal dimension, the longitude and latitude of the DBS are obtained by exhaustively searching for all the candidate locations that minimize the latency ratio of users that are associated with the DBS. Specifically,

Fist, in the horizontal dimension, we divide the coverage area into a number of locations with the same size. Denote $\mathcal{K}$ as the set of these locations and $k$ as the index of these locations. These locations would be the candidate locations that the DBS can be placed in the horizontal dimension (note that the longitude and latitude of the DBS can be obtained based on the corresponding location index).

Second, in the vertical dimension, find user $\bar{i}$ by calculating

$$\bar{i} = \arg\min_i \left\{ -10 \lg[(2^{\frac{T_i}{\beta^D} - 1} - 1)\frac{\sigma^2}{P^D}] \,|\, i \in \mathcal{I}_1 \right\}. \qquad (4.55)$$

Then, we set the flying height of the DBS as $h_{\bar{i}}^*$. Based on Lemma 1, we can conclude that the pathloss requirements (i.e., data rate requirements) of users located within the coverage area of the DBS can always be satisfied.

3) We exhaustively search all candidate locations in the horizontal dimension with the flying height of $h_{\bar{i}}^*$. The optimal location index $k^*$ of the DBS will be the one

which incurs the minimum value of $\sum_{i=1}^{|\mathcal{I}_1|} \frac{\lambda_i v_i}{\iota_i}$, i.e.,

$$k^* = \arg\min_k \left\{ \sum_{i=1}^{|\mathcal{I}_1|} \frac{\lambda_i v_i}{\iota_i} \mid k \in \mathcal{K} \right\}. \tag{4.56}$$

The joint DBS placement, bandwidth allocation and user association algorithm to solve the primal problem P0-a is embodied in Algorithm 1. In Line 1, we initialize the 3D location of the DBS. In Line 3, given the location, we obtain the bandwidth allocation and user association by solving problem P1-a. Given the bandwidth allocation and user association, Lines 4-5 determine the altitude of the DBS, while Lines 6-10 calculate the horizontal location of the DBS. We repeat Lines 3-10 until the algorithm converges.

The complexity of Step 3 is $O(|\mathcal{I}|^3)$; that of Steps 4-5 is $O(|\mathcal{I}|)$; that of Steps 6-8 is $O(|\mathcal{I}||\mathcal{K}|)$; that of Step 9 is also $O(|\mathcal{I}||\mathcal{K}|)$ and they can repeat for at most $O(|\mathcal{K}|)$ times. Thus, the complexity of Algorithm 2 is $O(|\mathcal{I}|^3 + |\mathcal{K}|^2 |\mathcal{I}|)$.

---

**Algorithm 2:**

---

**1** Initialize the location of the DBS $x$, $y$, $h$.

**2** **while** *the value of* (4.24) *decreases* **do**

**3** $\quad$ Compute $\theta_i$, $\beta^M$ and $\beta^D$ by solving problem **P1-a**;

**4** $\quad$ Identify user $\bar{i}$, where $\bar{i} = \arg\min\limits_{i} \left\{ -10\lg[(2^{\frac{T_i}{\beta^D}-1} - 1)\frac{\sigma^2}{P^D}] \mid i \in \mathcal{I}_1 \right\}$.

**5** $\quad$ Let the flying height of the DBS $h = h_{\bar{i}}^*$;

**6** $\quad$ **for** $k = 1$ *to* $|\mathcal{K}|$ **do**

**7** $\quad\quad$ Calculate the value of (4.24) in each iteration $k$;

**8** $\quad$ **end**

**9** $\quad$ Obtain horizontal location index $k^*$ based on (4.56);

**10** $\quad$ Calculate $x$, $y$ accordingly and let $h = h_{\bar{i}}^*$.

**11** **end**

---

## 4.4    Numerical Results

We next present numerical results to demonstrate the effectiveness of our proposed algorithm. We consider an area with the size of 500 $m$ by 500 $m$. The locations of the ground users follow the spatial Poisson point process with density of $\lambda_1 = 400$ $users/km^2$. The size of each location $k$ is 10 $m$ by 10 $m$. Users' data rate requirements are generated based on the Poisson distribution with the expectation of 50 $Kbps$. Other parameters are given in Table 4.2. MATLAB R2019a is used to run the simulations, which are run on a macbook laptop with Quad-Core intel Core i5-8257U and 8 GB RAM. We repeat each simulation five times to obtain the average value. Table 4.1 shows the runtime of each scheme where the number of users are set to 100 and 200, respectively. The other parameters are the same as shown in Table 4.2. We can see the proposed algorithm takes longer time to converge since a dynamic user association and bandwidth allocation policy is utilized to achieve better performance. The runtime of the 'Stationary DBS' scheme is longer than the 'MBS only' scheme because the bandwidth allocation and user association is the same as our proposed algorithm. While in the 'MBS only' scheme, all the bandwidth are allocated to the MBS and all the users are associated with the MBS.

**Table 4.1** Runtime Experiment Results

| Algorithms | 100 users | 200 users |
| --- | --- | --- |
|  | time (sec) | time (sec) |
| Proposed Algorithm | 2.93 | 4.62 |
| Stationary DBS | 1.13 | 1.85 |
| MBS only | 0.91 | 1.47 |

Next, we compare the performance of our algorithm with the following two schemes: 1) Stationary DBS, where the DBS is placed at the geometrical center with the flying height $h = 30m$. Meanwhile, the bandwidth allocation and user association

policy are optimized based on our proposed approach. 2) MBS only, where no DBS is deployed to assist the MBS in the existing cellular network. In this scheme, all the bandwidth is allocated to the MBS and all users are associated with the MBS.

**Table 4.2** Simulation Parameters II

| Parameters | Definitions | Values |
|---|---|---|
| $a$ | Environment parameter | 9.61 |
| $b$ | Environment parameter | 0.16 |
| $\eta_{LoS}$ | Average additional pathloss of LoS | $1\ dB$ |
| $\eta_{NLoS}$ | Average additional pathloss of NLoS | $20\ dB$ |
| $f$ | Carrier frequency | $2\ GHz$ |
| $\sigma^2$ | Noise power | $-140\ dBm$ |
| $B$ | Total available bandwidth | $20\ MHz$ |
| $P^D$ | Transmit power of DBS | $0.5\ W$ |
| $P^M$ | Transmit power of MBS | $2\ W$ |
| $\lambda_i$ | Arrival rate of user $i$ | $0.1\ request/s$ |
| $v_i$ | Average traffic size of user $i$ | $100\ Kb$ |
| $\epsilon$ | Latency ratio requirement | 2 |

Figure 4.2 illustrates how the total number of users affects the average latency ratio. It is easy to see that with the increase of the number of users, the average latency ratio increases in all schemes. The proposed approach achieves the best performance (i.e., lowest average latency ratio) as compared to the other two algorithms. The following two factors explain the reason: 1) The average latency ratio can be reduced by associating users to the DBS (which has better channel condition as compared to associating with the MBS). 2) It can also be reduced by
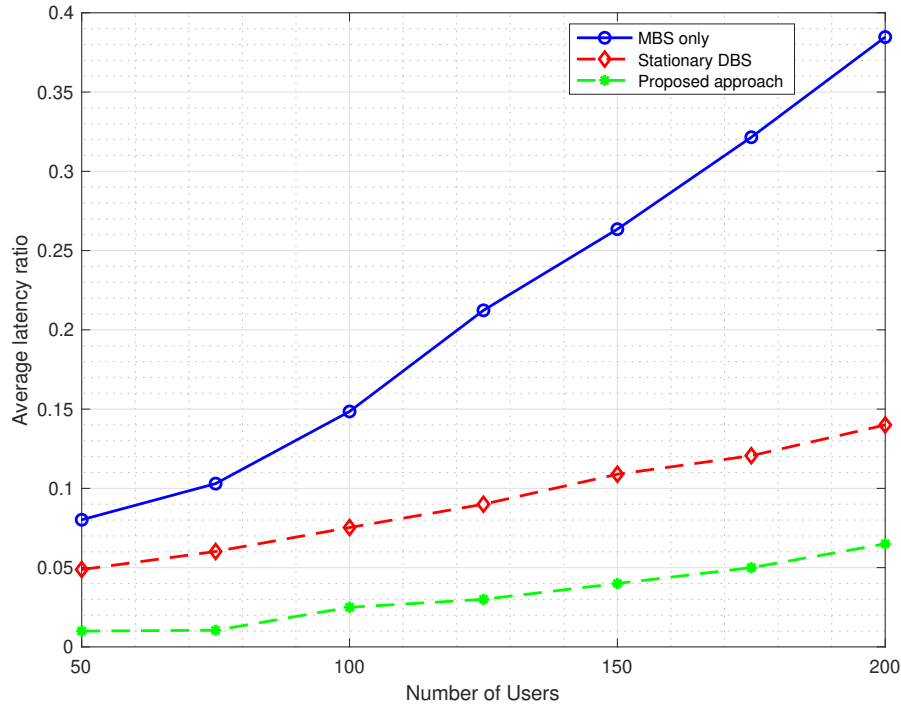
**Figure 4.2** The average latency ratio and number of users.

flexibly adjusting the DBS's location to those which incur lower average latency ratio (as compared to the 'Stationary DBS' scheme).

Figure 4.3 illustrates the transmission power of the DBS versus the average latency ratio. From Figure 4.3, we can see that the average latency ratio of the 'Stationary DBS' scheme and that of our designed approach decrease as the transmission power of DBS increases because the increase of transmission power will improve the achievable rate of the access link and thus reduce the average latency ratio of users associated with the DBS. The average latency ratio of the 'MBS only' scheme stays constant since no DBS is deployed in this case.

Figures 4.4 and 4.5 show how the transmission power of the MBS and the total available bandwidth affect the average latency ratio, respectively. In both figures, we can observe that the average latency ratio decreases as the amount of resource increases. In Figure 4.4, the average latency ratio of the 'MBS only' scheme reduces
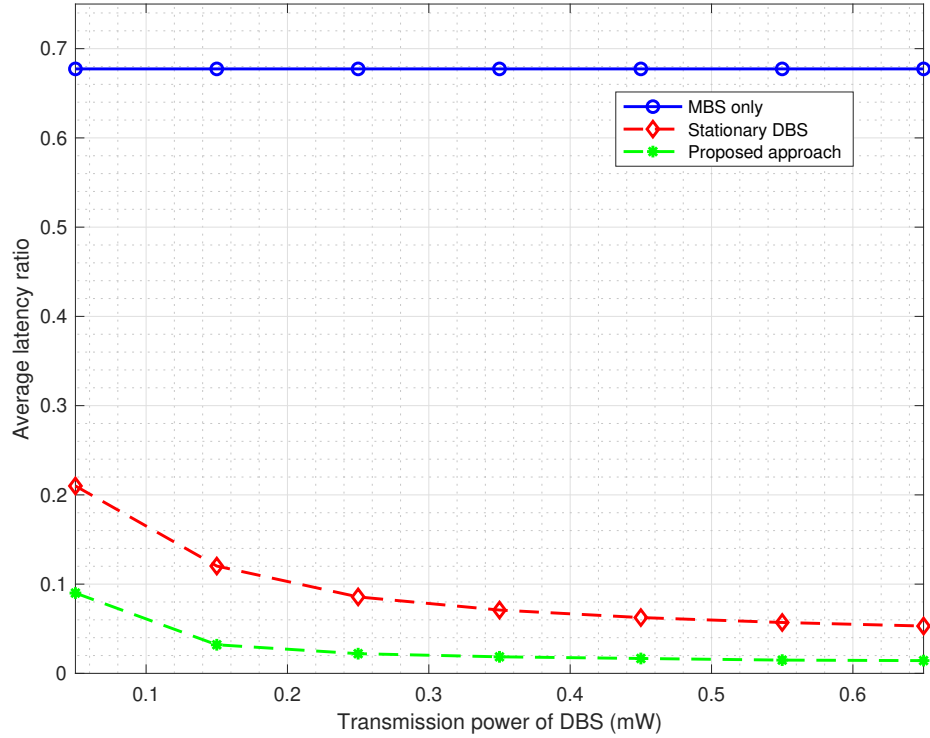
**Figure 4.3** The average latency ratio versus transmission power of DBS.

significantly as the transmission power of MBS increases because all the users are associated with the MBS in this case and the increase of transmission power will affect all users. However, in the other two schemes where a DBS is deployed, the decrease is much less remarkable because the majority of users are associated with the DBS (since it provides a better channel condition) and the increase of transmission power of MBS does not influence such users.

From Figure 4.6, we can observe that with the increase of the average traffic size, the average latency ratio increases in all schemes because the service time of each user increases, thus resulting in a larger latency ratio. Both schemes with DBSs outperform the 'MBS only' scheme since a better channel connection is provided. Furthermore, our proposed scheme achieves better performance as compared with

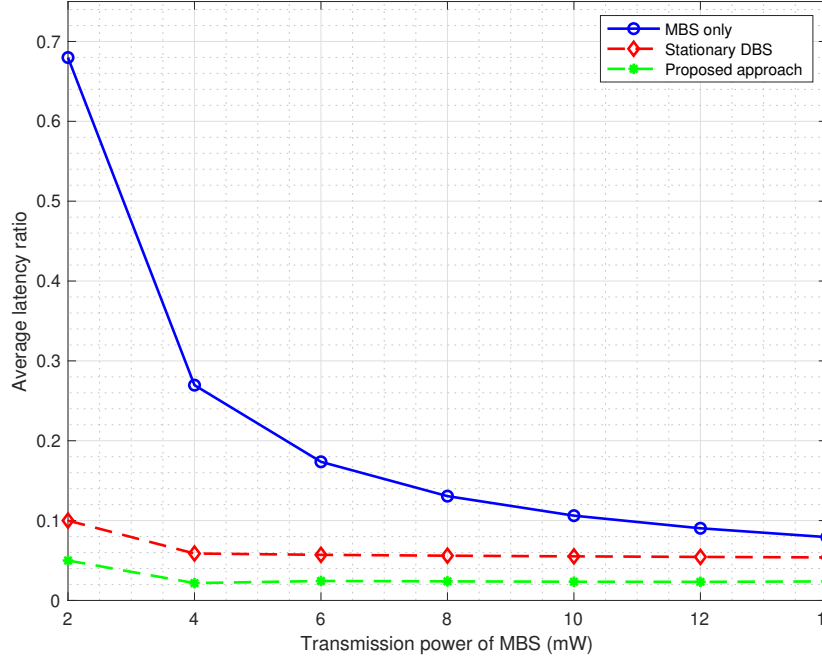**Figure 4.4** The average latency ratio versus transmission power of MBS.
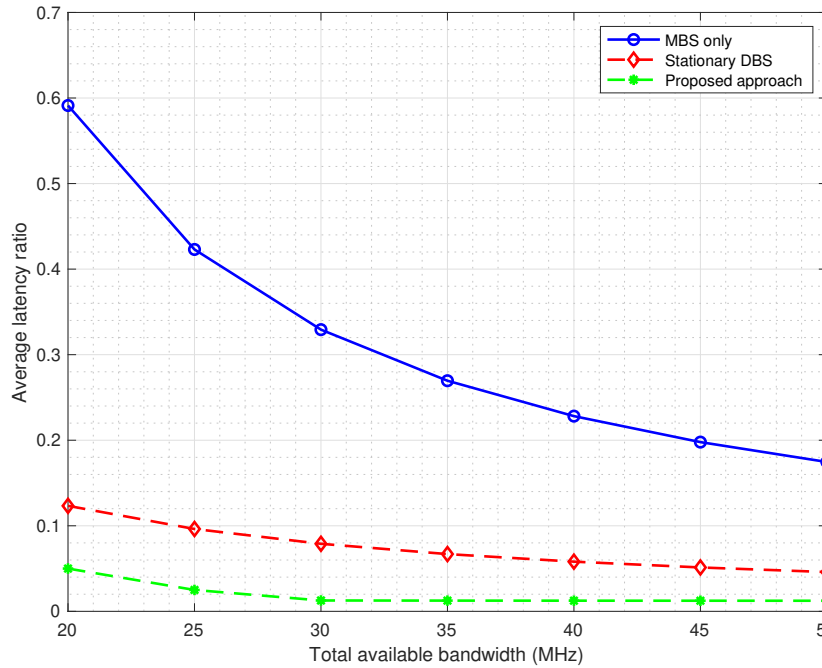


**Figure 4.5** The average latency ratio versus total available bandwidth.
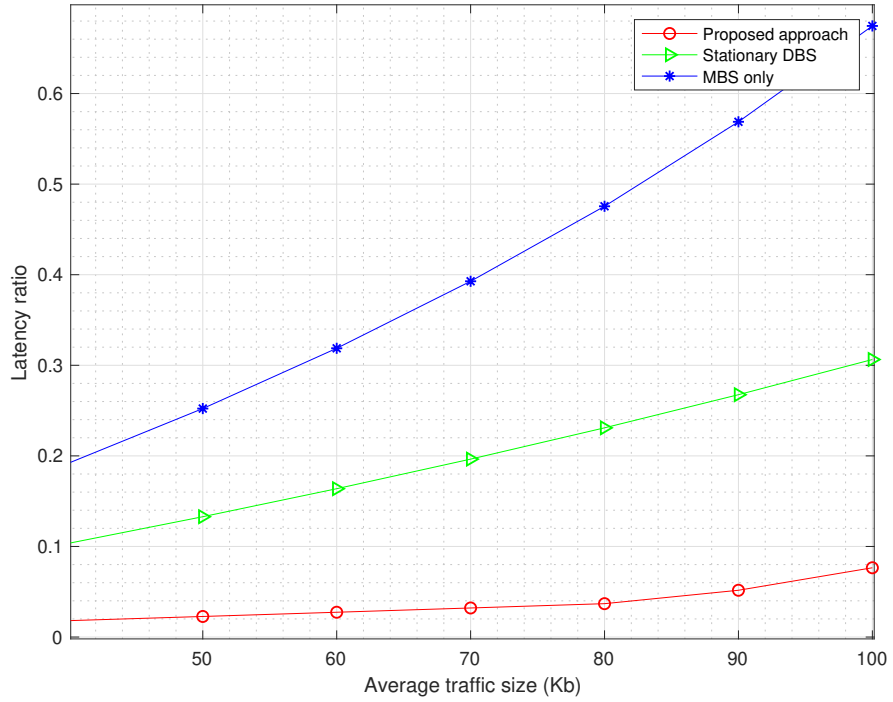
**Figure 4.6** The average latency ratio versus the average traffic size.

the 'Stationary DBS' scheme because the latency can be reduced by adjusting the location of the DBS and the resource allocation between the MBS and DBS.

# CHAPTER 5

# TETHERED-UAV ASSISTED HETEROGENEOUS NETWORK

In this chapter, we propose to prolong a UAV's flight time by connecting the UAV through a tether with a ground charging station (GCS). The GCS can provide a stable power supply and a wired backhaul link (when Internet is accessible for the GCS) while maintaining UAV's maneuverability to a certain extent.

## 5.1   System Model
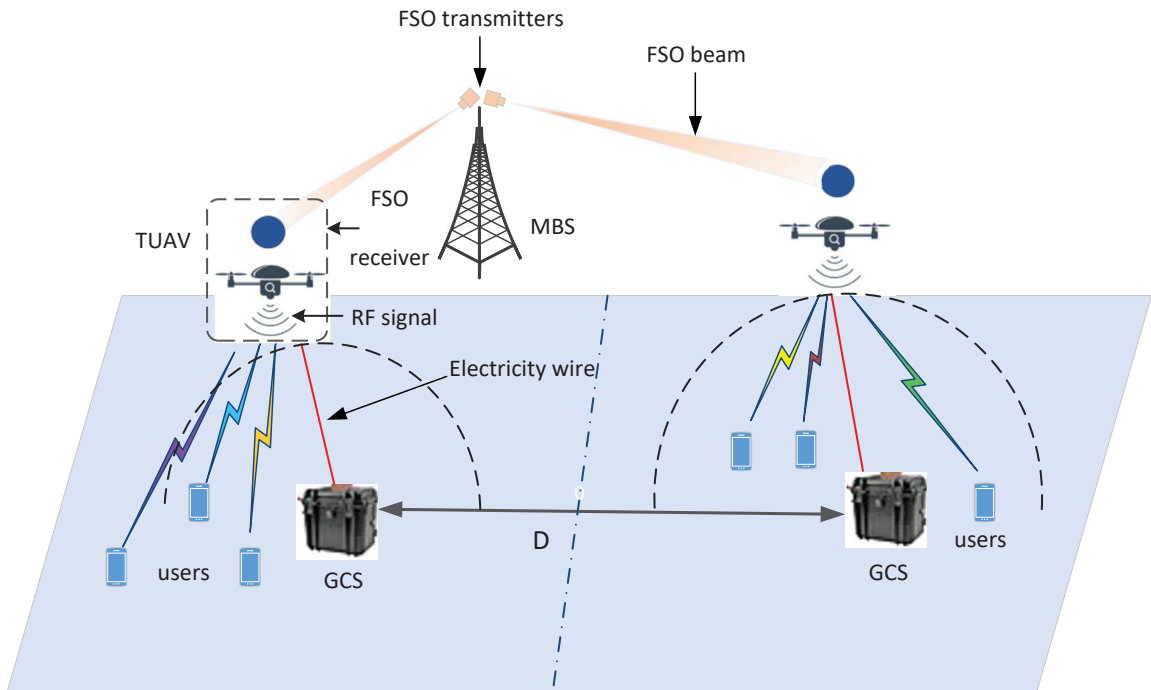


**Figure 5.1** TUAV-assisted heterogeneous network.

As shown in Figure 5.1, we consider a TUAV-assisted heterogeneous network where the TUAVs work as relay nodes between the MBS and ground users. Our proposed framework can theoretically work for unlimited time while maintaining UAV's maneuverability to a certain extent as compared with deploying untethered

UAV. Each aerial UAV is connected to a GCS to obtain the power supply. To avoid interference among users, the frequency division multiple access (FDMA) mode is employed. The channel pathloss model, the conditions of avoiding tangling among TUAVs and the FSO-based capacity model are presented in this section. To achieve the maximum system throughput, an optimization problem subject to the user QoS requirements, limited available resource and tangling avoidance is formulated.

### 5.1.1 Pathloss Model of the Access Link

Denote the set of users and the set of TUAVs as $\mathcal{I}$ and $\mathcal{J}$, respectively. We consider a Cartesian coordinate system with ground user $i$, GCS $j$ and UAV $j$ located at $(x_i, y_i, 0)$, $q_j^G = (x_j^G, y_j^G, 0)$ and $q_j^U = (x_j^U, y_j^U, H_j)$, respectively. Note that each UAV is uniquely associated with a GCS. TUAV $j$ is assumed to fly at a fixed height $H_j$. Furthermore, we assume that the wireless channels in the access link are LoS-dominated. We do not constrain our application scenario to the rural area since our model can also be applied to temporary events (e.g., concerts and football matches) that are held in the urban area as long as the channels between users and UAVs are not blocked by surrounding buildings, i.e., LoS dominated. Obviously, it can also be applied to the rural area without high-rise buildings. Therefore, the down link pathloss from TUAV $j$ to ground user $i$ can be described by the free-space path loss model [43]

$$\xi_{ij} = \beta_0 d_{ij}^2 = \beta_0[(x_i - x_j^U)^2 + (y_i - y_j^U)^2 + H_j^2], \tag{5.1}$$

where $\beta_0$ denotes the pathloss at the reference distance $d = 1\,m$. With the assumption of perfect modulation, the maximum achievable data rate between ground user $i$ and TUAV $j$ can be expressed as

$$R_{ij} = b_i \log_2(1 + \frac{p_i}{\xi_{ij}\sigma^2}), \tag{5.2}$$

where $b_i$ and $p_i$ are the amount of bandwidth and transmit power allocated for user $i$, respectively. $\sigma^2$ denotes the environment noise power.

**Lemma 4.** *Denote $L_1$ and $L_2$ as the tether length of TUAV 1 and TUAV 2, respectively, and $\theta_1^{th}$ and $\theta_2^{th}$ as the minimum allowed inclination angle of TUAV 1 and TUAV 2, respectively. Then, the minimum distance between TUAV 1 and TUAV 2 to avoid tangling is $D^{th} = \sqrt{L_1^2 - (L_2 \sin \theta_2^{th})^2} + L_2 \cos \theta_2^{th}$.*

*Proof.* Figure 5.2 illustrates the critical point to avoid tangling between two TUAVs, i.e., the two TUAVs might tangle with each other if the distance between them is smaller the minimum value. $O_1$ and $O_2$ are the locations of GCSs of TUAV 1 and TUAV 2, respectively, and $A'$ and $B'$ are the projections of $A$ and $B$ onto line segment $O_1 O_2$, respectively. The circle stands for the area that the TUAV can reach. $\angle BO_1 B' = \theta_1^{th}$, $\angle AO_2 A' = \theta_1^{th}$, $BO_1 = L_1$, and $AO_2 = L_2$. Then, the minimum distance to avoid tangling between two TUAVs can be easily obtained through (5.3). Here, we demonstrate the case where $L_1 \sin \theta_2^{th} < L_2 \sin \theta_2^{th}$. The case $L_1 \sin \theta_2^{th} \geq L_2 \sin \theta_2^{th}$ can be proven similarly. Thus,

$$
\begin{aligned}
D^{th} = O_1 O_2 &= O_1 A' + A' O_2 \\
&= \sqrt{L_1^2 - (L_2 \sin \theta_2^{th})^2} + L_2 \cos \theta_2^{th}.
\end{aligned}
\tag{5.3}
$$

Note that this conclusion can be easily extended to the case where multiple TUAVs are deployed, i.e., any two of the deployed TUAVs should meet the requirements shown in Lemma 4. Hence, we only show the special case of two TUAVs in Lemma 4 because the conclusion can also be applied to the case of multiple TUAVs. $\qquad\square$
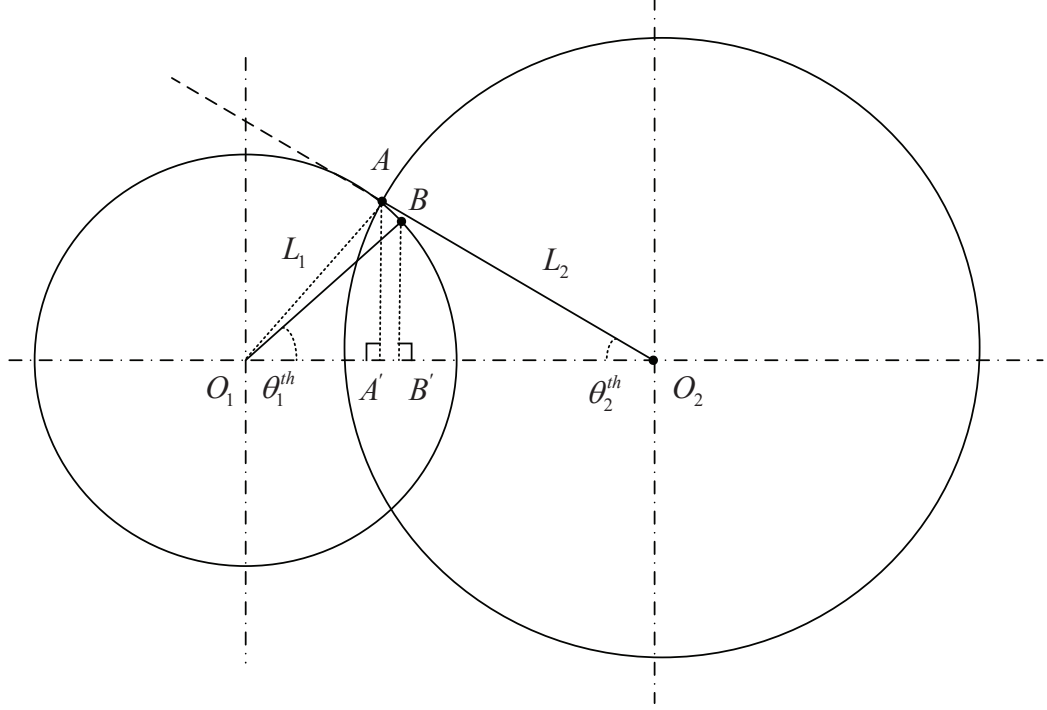
**Figure 5.2** Minimum distance between two TUAVs to avoid tangling.

### 5.1.2 FSO Capacity Model

We adopt FSO to facilitate the backhaul link, whose capacity can be calculated by [5]:

$$C = \frac{P_t \eta_t \eta_r 10^{-\frac{L_{atm}}{10}} 10^{-\frac{L_{geo}}{10}}}{E_p N_b}, \tag{5.4}$$

where $P_t$ is the transmission power of the laser, and $\eta_t$ and $\eta_r$ denote the transmitting efficiency and receiving efficiency, respectively. $E_p = h_p c/\lambda_c$ is the photon energy. $\lambda_c$ is the carrier wavelength, $h_p$ denotes Plank's constant. $N_b$ reflects the receiver sensitivity (photons/bit). $L_{geo} = 10 \log(\frac{\pi r^2}{\pi(\psi_t l/2)^2})$ is the geometrical loss in dB, $l$ is the distance between the laser transmitter and receiver in $Km$, $r$ is the radius of the receiver's aperture in $m$, and $\psi_t$ denotes the transmitting divergence angle. $L_{atm} = \frac{17}{\Delta}(\frac{\lambda}{550nm})^{-\delta}$ stands for the atmospheric attenuation caused by bad weather conditions, where $L_{atm}$ is in dB/Km, $\delta$ is the size distribution of the scattering particles, and $\Delta$ is the visibility in $Km$. The value of $\delta$ is determined by (3.9).

## 5.2 Problem Formulation

In this section, we try to maximize the sum rate of all users while meeting the QoS requirements of users, the limited available resource and tangling avoidance among TUAVs. Specifically, the problem can be formulated as follows,

$$\textbf{P0:} \quad \max_{\mathbf{q}_j^G, \mathbf{q}_j^U, b_i, p_i, u_{ij}} \quad \sum_{i=1}^{|\mathcal{I}|} \sum_{j=1}^{|\mathcal{J}|} R_{ij} u_{ij} \tag{5.5}$$

$$s.t. \quad \sum_{j=1}^{|\mathcal{J}|} R_{ij} u_{ij} \geq R_i^{th}, \forall i \in \mathcal{I}, \tag{5.6}$$

$$\sum_{i=1}^{|\mathcal{I}|} p_i u_{ij} \leq P_j^{max}, \forall j \in \mathcal{J}, \tag{5.7}$$

$$\sum_{i=1}^{|\mathcal{I}|} b_i \leq B, \tag{5.8}$$

$$||\mathbf{q}_j^G - \mathbf{q}_k^G|| \leq D^{th}, \forall j \neq k \in \mathcal{J}, \tag{5.9}$$

$$||\mathbf{q}_j^G - \mathbf{q}_j^U||^2 \leq L_j^2, \forall j \in \mathcal{J}, \tag{5.10}$$

$$\frac{H_j}{\sqrt{(x_j^U - x_j^G)^2 + (y_j^U - y_j^G)^2}} \geq \sin \theta_j^{th}, \forall j \in \mathcal{J}, \tag{5.11}$$

$$b_i \geq 0, \forall i \in \mathcal{I}, \tag{5.12}$$

$$p_i \geq 0, \forall i \in \mathcal{I}, \tag{5.13}$$

$$\sum_{j=1}^{|\mathcal{J}|} u_{ij} \leq 1, \tag{5.14}$$

$$u_{ij} = \{0, 1\}, \forall i \in \mathcal{I}, \forall j \in \mathcal{J}, \tag{5.15}$$

where $R_i^{th}$ denotes the data rate requirement of user $i$ and $P_j^{max}$ is the maximum transmission power of TUAV $j$. $B$ denotes the total available bandwidth. Constraints (5.7) and (5.8) stand for the resource limitations. Constraint (5.9) prevents tangling between TUAVs. Constraint (5.10) imposes the tether length limitation. Constraint (5.11) ensures that the tether inclination angles are above their minimum allowed values. Constraints (5.12) and (5.13) impose resources allocated to users to be non-

negative. Constraint (5.14) imposes one user to be associated to one TUAV at most. Constraint (5.15) imposes $u_i$ to be a binary variable. Note that we omit the constraint that the backhaul capacity should be larger or equal to the traffic in the access link since an FSO link can achieve a data rate of 1-2 Gbps in the range of 1-5 Km [5].

It is challenging to solve **P0** owing to the integer decision variables. Moreover, **P0** is also a non-convex programming problem since $R_{ij}$ is non-convex w.r.t. $\mathbf{q}_j^U$. Thus, we propose the Cyclic iterAtive TUAV placeMent, usEr association and Resource Allocation (CAMERA) algorithm to efficiently obtain suboptimal solutions of the formulated problem. In essence, we partition the decision variables into three blocks, i.e., the TUAV placement, user association and resource allocation. In each iteration, firstly, given the TUAVs' locations and user association policy, we obtain the optimal resource allocation and update the objective function value. Secondly, given the TUAVs' locations and resource allocation scheme, we update the user association policy. Thirdly, given the resource allocation scheme and user association policy, we determine the TUAVs' locations. This procedure is done iteratively until the convergence criterion is met.

## 5.3   Cyclic iterAtive TUAV placeMent, usEr association and Resource Allocation (CAMERA)

To make **P0** more tractable, we decouple the primal problem into three subproblems and optimize each subproblem alternately. We next discuss these three subproblems.

### 5.3.1   TUAV Placement

It is worth noting that in the TUAV placement problem, given the resource allocation scheme and user association policy, we need to not only determine the locations of the the UAVs but also the locations of GCSs. The TUAV placement problem can be expressed as

$$\textbf{P1:} \max_{\mathbf{q}_j^G, \mathbf{q}_j^U} \sum_{i=1}^{|\mathcal{I}|} \sum_{j=1}^{|\mathcal{J}|} R_{ij} u_{ij}$$

$$s.t. \quad \sum_{j=1}^{|\mathcal{J}|} R_{ij} u_{ij} \geq R_i^{th}, \forall i \in \mathcal{I}, \tag{5.16}$$

$$||\mathbf{q}_j^G - \mathbf{q}_k^G|| \leq D^{th}, \forall j \neq k \in \mathcal{J}, \tag{5.17}$$

$$(x_j^U - x_j^G)^2 + (y_j^U - y_j^G)^2 + H_j^2 \leq L_j^2, \forall j \in \mathcal{J}, \tag{5.18}$$

$$\frac{H_j}{\sqrt{(x_j^U - x_j^G)^2 + (y_j^U - y_j^G)^2}} \geq \sin \theta_j^{th}, \forall j \in \mathcal{J}. \tag{5.19}$$

Problem **P1** is still challenging since $R_{ij}$ is non-concave w.r.t. $\mathbf{q}_j^G$ and $\mathbf{q}_j^U$. To solve this problem, we try to first determine the locations of the GCSs and then obtain the locations of the UAVs.

**Lemma 5.** *Assume the ground users follow a uniform distribution [44, 45], the optimal horizontal location of the UAV that minimizes the average path loss of all users is the geometrical center of the area.*

*Proof.* Since the ground users are uniformly scattered in the square area shown in Figure 5.1, the probability distribution function (pdf) of a given user in location $(x, y, 0)$ is

$$f(x, y) = \begin{cases} \frac{1}{4LW}, & \text{if } |x| \leq L, |y| \leq W, \\ 0, & \text{otherwise}, \end{cases} \tag{5.20}$$

where $2L$ and $2W$ are the length and width of the area, respectively. Thus, the average path loss of all users can be calculated by

$$E(\xi) = \iint\limits_{|x| \le L, |y| \le W} (\frac{1}{4LW} \cdot \xi) \, dxdy \tag{5.21}$$

$$\stackrel{a}{=} \iint\limits_{|x| \le L, |y| \le W} \{\frac{\beta_0}{4LW}[H^2 + (x - x^U)^2 + (y - y^U)^2]\} \, dxdy$$

$$= \beta_0[H^2 + \frac{1}{3}L^2 + \frac{1}{3}W^2 + (x^U)^2 + (y^U)^2] \tag{5.22}$$

$$\stackrel{b}{\ge} \beta_0(H^2 + \frac{1}{3}L^2 + \frac{1}{3}W^2)$$

where step (a) is derived by substituting Equation (5.1) into Equation (5.21), and the equality condition in step (b) holds when $x^U = 0$ and $y^U = 0$ (i.e., the geometrical center of the square area). We can observe from (5.22) that the average path loss of all users is an increasing function of the distance between the UAV and the geometrical center of the square area. $\square$

Based on Lemma 5, we place each GCS around the geometrical center of the area by setting the distance between every two successive GCSs to be $D^{th}$ as shown in Figure 5.3 for an example with 4 TUAVs. It is worth noting that Lemma 5 is derived based on the intuition that a smaller pathloss yields a higher data rate. We place the GCSs based on Lemma 5 to ensure that the aerial UAVs can reach the geometrical centers. Note that the aerial UAVs may not be able to be deployed at the geometrical centers if the GCSs are placed too far away from the geometrical centers as they are confined by the tether. Also, the optimal locations of the aerial UAVs may not necessarily be the geometrical centers; they are further adjusted to maximize the sum rate of all users by searching the candidate locations in the horizontal plane.
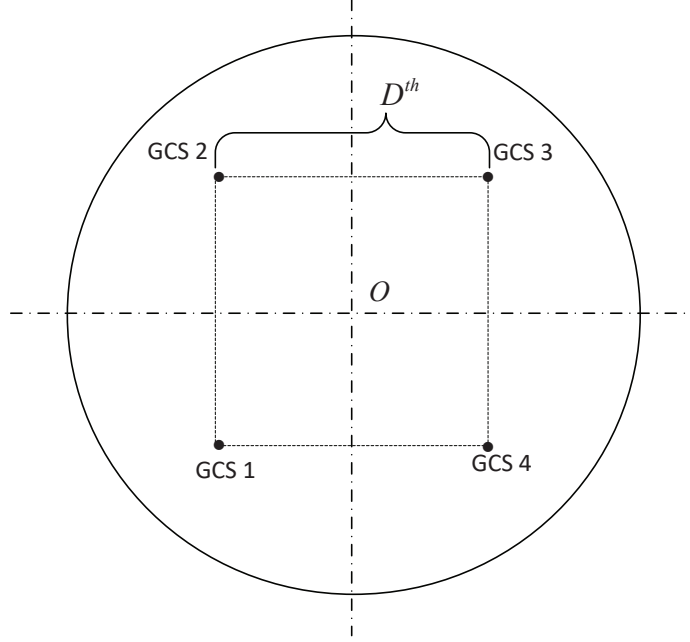
**Figure 5.3** An example of GCS placement.

Given locations of the GCSs (i.e., given $x_j^G$ and $y_j^G$), **P1** can be rewritten as

$$\textbf{P1-a:} \ \max_{\mathbf{q}^U} \ \sum_{i=1}^{|\mathcal{I}|} \sum_{j=1}^{|\mathcal{J}|} R_{ij} u_{ij}$$

$$s.t. \quad (x_j^U - x_i)^2 + (y_j^U - y_i)^2$$

$$\leq \frac{p_i}{\sigma^2 \beta_0 (2^{R_i^{th}/b_i} - 1)} - H_j^2, \forall i \in \mathcal{I}, \tag{5.23}$$

$$(x_j^U - x_j^G)^2 + (y_j^U - y_j^G)^2 \leq L_j^2 - H_j^2, \forall j \in \mathcal{J}, \tag{5.24}$$

$$(x_j^U - x_j^G)^2 + (y_j^U - y_j^G)^2 \leq \frac{H_j^2}{\sin^2 \theta_j^{th}}, \forall j \in \mathcal{J}. \tag{5.25}$$

Note that in **P1-a**, variables $q_1^U$ to $q_{|\mathcal{J}|}^U$ are independent of each other. Thus, we can solve problem **P1-a** by solving $|\mathcal{J}|$ independent subproblems, i.e.,

$$\textbf{P1-b:}\ \max_{q_j^U}\ \sum_{i=1}^{|\mathcal{I}|} R_{ij} u_{ij}$$

$$\text{s.t.}\quad (x_j^U - x_i)^2 + (y_j^U - y_i)^2$$

$$\leq \frac{p_i}{\sigma^2 \beta_0 (2^{R_i^{th}/b_i} - 1)} - H_j^2, \forall i \in \mathcal{I}, \tag{5.26}$$

$$(x_j^U - x_j^G)^2 + (y_j^U - y_j^G)^2 \leq L_j^2 - H_j^2, \tag{5.27}$$

$$(x_j^U - x_j^G)^2 + (y_j^U - y_j^G)^2 \leq (\frac{H_j}{\sin \theta_j^{th}})^2. \tag{5.28}$$

**Lemma 6.** *Problem **P1-b** is neither a convex nor a concave optimization problem.*

*Proof.* Note that **P1-b** can be proven to be neither a convex nor a concave optimization problem if $R_{ij}$ is neither a convex nor a concave function w.r.t. $x_j^U$ or $y_j^U$. Since $R_{ij}$ shares the same convexity with function $f = \log(1 + 1/(x^2 + y^2 + H^2))$, we next study the convexity of $f$ instead of $R_{ij}$ for simplicity. Note that $f$ can be rewritten as a composition function of $x$ and $y$, i.e.,

$$f = h(g(x, y)), \tag{5.29}$$

where $h(x) = \log(1 + \frac{1}{x})$ and $g(x, y) = x^2 + y^2 + H^2$. The second derivative of the composition function $f = h(g(x, y))$ can be calculated by

$$f''(x) = h''(g(x))g'(x)^2 + h'(g(x))g''(x)$$
$$= \frac{2\left(3x^4 + (2y^2 + 2h^2 + 1)x^2 - y^4 - (2h^2 + 1)y^2 - h^4 - h^2\right)}{(x^2 + y^2 + h^2)^2 (x^2 + y^2 + h^2 + 1)^2}.$$

Note that $f'' > 0$ (i.e., $f$ is a convex function) when the value of $x$ is sufficiently large and that of $y$ is sufficiently small, and $f'' < 0$ (i.e., $f$ is a concave function) when the value of $x$ is sufficiently small and that of $y$ is sufficiently large, thus leading to **P1-b** being neither a convex nor a concave optimization problem. □

To solve **P1-b**, we first divide a given area into several candidate locations with the same size and then obtain the UAV's location by utilizing the exhaustive method. UAV $j$ is finally placed at the location which incurs the maximum value of the objective function (i.e., the sum rate). Note that the number of the squares (i.e., candidate locations of the aerial UAVs) is limited; the complexity of our method therefore incurs limited complexity. Specifically,

First, we divide the coverage area into a number of locations with the same size. Denote $\mathcal{K}$ as the set of these locations and $k$ as the index of these locations. These locations would be the candidate locations that the UAV can be placed (note that the longitude and latitude of the DBS can be obtained based on the corresponding location index).

Second, we exhaustively search all candidate locations with the fixed flying height of $H_j$. The optimal location index $k^*$ will be the one which incurs the maximum value of $\sum_{i=1}^{|\mathcal{I}|} R_{ij} u_{ij}$, i.e.,

$$k^* = \arg\max_k \left\{ \sum_{i=1}^{|\mathcal{I}|} R_{ij} u_{ij} \mid (5.26), (5.27), (5.28), k \in \mathcal{K} \right\}. \qquad (5.30)$$

### 5.3.2 Resource Allocation

Given the TUAVs' locations and user association policy, we try to maximize the throughput in the access link via optimizing the resource allocation. The primal

problem can thus be reduced to

$$\textbf{P2:} \max_{b_i, p_i} \sum_{i=1}^{|\mathcal{I}|} \sum_{j=1}^{|\mathcal{J}|} R_{ij} u_{ij}$$

$$s.t. \quad \sum_{j=1}^{|\mathcal{J}|} R_{ij} u_{ij} \geq R_i^{th}, \forall i \in \mathcal{I}, \tag{5.31}$$

$$\sum_{i=1}^{|\mathcal{I}|} p_i u_{ij} \leq P_j^{max}, \forall j \in \mathcal{J}, \tag{5.32}$$

$$\sum_{i=1}^{|\mathcal{I}|} b_i \leq B, \tag{5.33}$$

$$b_i \geq 0, \forall i \in \mathcal{I}, \tag{5.34}$$

$$p_i \geq 0, \forall i \in \mathcal{I}. \tag{5.35}$$

**Lemma 7.** *P2 is a concave optimization problem.*

*Proof.* We can observe that **P2** is a concave optimization problem if $R_{ij}$ is a concave function of $b_i$ and $p_i$ since Constraints (5.32), (5.33), (5.34) and (5.35) are all linear functions. It is worth noting here that the summation in the objective function does not influence the convexity of **P2**. The Hessian matrix of $R_{ij}$ w.r.t. $b_i$ and $p_i$ can be derived as

$$\nabla^2 R_{ij} = \begin{bmatrix} 0, & \dfrac{1}{(p_i + \alpha_{ij}) \ln 2} \\ \dfrac{1}{(p_i + \alpha_{ij}) \ln 2}, & -\dfrac{b_i}{(p_i + \alpha_{ij})^2 \ln 2} \end{bmatrix}, \tag{5.36}$$

where $\alpha_{ij} = \sigma^2 \beta_0 ((x_j^U - x_i)^2 + (y_j^U - y_i)^2 + H_j^2)$. Since $b_i$, $p_i$ and $\alpha_{ij}$ are positive, $\nabla^2 R_{ij}$ is negative semidefinite, which indicates that $R_{ij}$ is concave w.r.t. $b_i$ and $p_i$. $\square$

Since **P2** has been proven to be a concave optimization problem, we can utilize CVX or CPLEX to obtain its optimal solutions.

### 5.3.3 User Association

In the user association problem, given the TUAVs' locations and resource allocation, we determine the user association policy to maximize the sum rate of all users by solving the following optimization problem:

$$\textbf{P3:} \max_{u_{ij}} \sum_{i=1}^{|\mathcal{I}|} \sum_{j=1}^{|\mathcal{J}|} R_{ij} u_{ij}$$

$$s.t. \quad \sum_{j=1}^{|\mathcal{J}|} R_{ij} u_{ij} \geq R_i^{th}, \forall i \in \mathcal{I}, \tag{5.37}$$

$$\sum_{i=1}^{|\mathcal{I}|} p_i u_{ij} \leq P_j^{max}, \forall j \in \mathcal{J}, \tag{5.38}$$

$$\sum_{j=1}^{|\mathcal{J}|} u_{ij} \leq 1, \tag{5.39}$$

$$u_{ij} = \{0, 1\}, \forall i \in \mathcal{I}, \forall j \in \mathcal{J}. \tag{5.40}$$

Note that **P3** is a Generalized Assignment Problem (GAP) problem, where user $i$ and TUAV $j$ are mapped to item $i$ and knapsack $j$, respectively. Thus, $R_{ij}$ is the profit of item $i$ if assigned to knapsack $j$, $p_i$ is the weight of item $i$ and $P_j^{max}$ is the capacity of knapsack $j$. The optimal solution of **P3** can be obtained through depth-first branch-and-bound method [46–48].

We summarize the steps of the CAMERA algorithm in Algorithm 3. Line 1 initializes all parameters. The complexity of Line 3 is $O(|\mathcal{K}||J|)$, that of Line 4 is $O(|\mathcal{I}|)$, that of Line 5 is $O(|\mathcal{I}||\mathcal{J}|^2)$ in the worst case [48], Lines 3-5 can repeat for no more than $|\mathcal{K}|$ times. Hence, the complexity of CAMERA is $O(|\mathcal{K}|^2|\mathcal{J}| + |\mathcal{K}||\mathcal{I}||\mathcal{J}|^2)$.

---
**Algorithm 3:**

---

**1** Initialize $\mathbf{q}^{G^{(0)}}$, $\mathbf{q}^{U^{(0)}}$, $b_i^{(0)}$, $p_i^{(0)}$, $u_{ij}^{(0)}$. Set the iteration number n=1.

**2 while** *the value of* (5.5) *increases* **do**

**3** $\quad$ Given $b_i^{(n-1)}$, $p_i^{(n-1)}$ and $u_{ij}^{(n-1)}$, obtain $\mathbf{q}^{G^{(n)}}$ and $\mathbf{q}^{U^{(n)}}$ by solving **P1**;

**4** $\quad$ Given $\mathbf{q}^{G^{(n)}}$, $\mathbf{q}^{U^{(n)}}$ and $u_{ij}^{(n-1)}$, acquire the optimal $b_i^{(n)}$ and $p_i^{(n)}$ by solving **P2**;

**5** $\quad$ Given $\mathbf{q}^{G^{(n)}}$, $\mathbf{q}^{U^{(n)}}$, $b_i^{(n)}$ and $p_i^{(n)}$, obtain the optimal $u_{ij}^{(n)}$ by solving **P3**;

**6** $\quad$ Set the iteration number n=n+1;

**7 end**

**8** Output $\mathbf{q}^{G*} = \mathbf{q}^{G^{(n)}}$, $\mathbf{q}^{U*} = \mathbf{q}^{U^{(n)}}$, $b_i^* = b_i^{(n)}$, $p_i^* = p_i^{(n)}$ and $u_{ij}^* = u_{ij}^{(n)}$.

---

## 5.4 Simulations

In this section, we provide numerical results to evaluate the performance of CAMERA. Here, two TUAVs are deployed over a rectangle area with the size of 1000 $m$ × 500 $m$. The flying heights of two TUAVs are $H_1 = H_2 = 100$ $m$. The ground users are uniformly distributed in the area. The size of each location $k$ in the given area is 10 $m$ by 10 $m$. Users' data rate requirements are generated based on the Poisson distribution with the expectation of 50 Kbps. For simplicity, we summarize other simulation parameters in Table 5.1. Next, we compare the performance of CAMERA with the following two schemes: 1) Stationary DBS, where the DBS is placed at the geometrical center with the flying height $h = 100m$. Meanwhile, the bandwidth is equally allocated to all users. 2) MBS only, where no DBS is deployed to assist the MBS in the existing cellular network. In this scheme, all users are directly connected to the MBS without a relay with equally allocated resource. The MBS is located at $(500, 500)$.

**Table 5.1** Simulation Parameters III

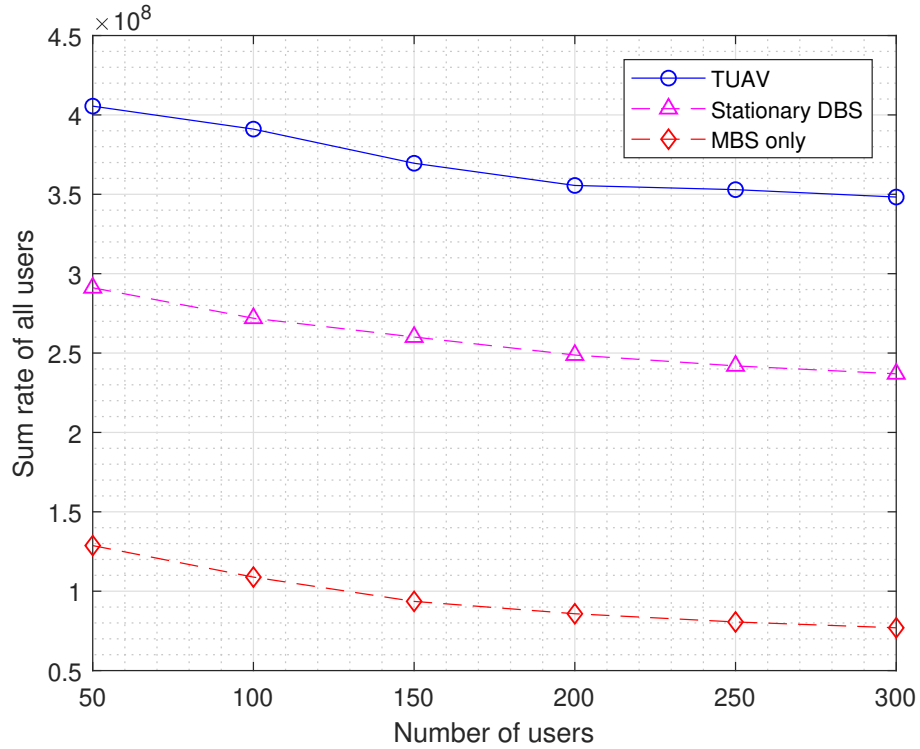| Parameters | Definition | Value |
|---|---|---|
| $\sigma^2$ | Noise power | -140 $dBm$ |
| $B$ | Total available bandwidth | 20 $MHz$ |
| $P^D$ | Transmit power of DBS | 0.5 $mW$ |
| $P^M$ | Transmit power of MBS | 1 $mW$ |
| $P_j^{max}$ | Transmit power of TUAV 1, 2 | 0.5 $mW$ |
| $\theta_j^{th}$ | Minimum allowed inclination angle | $\pi/3$ $rad$ |
| $L_j$ | Tether length of TUAV 1, 2 | 120 $m$ |
| $D^{th}$ | Minimum distance to avoid tangling | 120 $m$ |



**Figure 5.4** Sum rate of all users versus number of users.

Figure 5.4 shows the sum rate of all users of the TUAV scheme, stationary DBS scheme and MBS only scheme, respectively. From Figure 5.4, we can see the sum rate of all users of our proposed approach outperforms that of the stationary DBS approach by nearly 50%. Both schemes with relays outperform the 'MBS only' scheme since a better channel condition is provided. Furthermore, as shown in the figure, the sum rate of all approaches decreases as the number of users increases. This is because as the number of users increases, more resources have to be allocated to users that experience worse channel conditions, and thus less resources are left for the users that have better channel conditions. To achieve the maximal sum rate, all the remaining resources (after user QoS requirements are met) should be allocated to the user that has the best channel condition. With the increase of users, more resources need to be allocated to the newly emerging users to guarantee their QoS, thus leading to a decrease of the sum rate of all users.
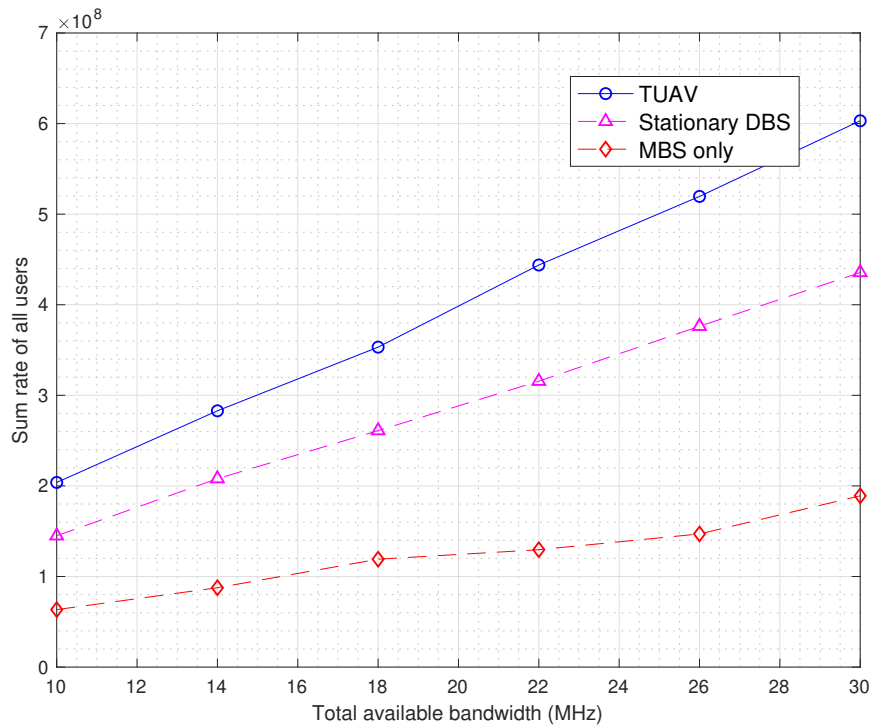


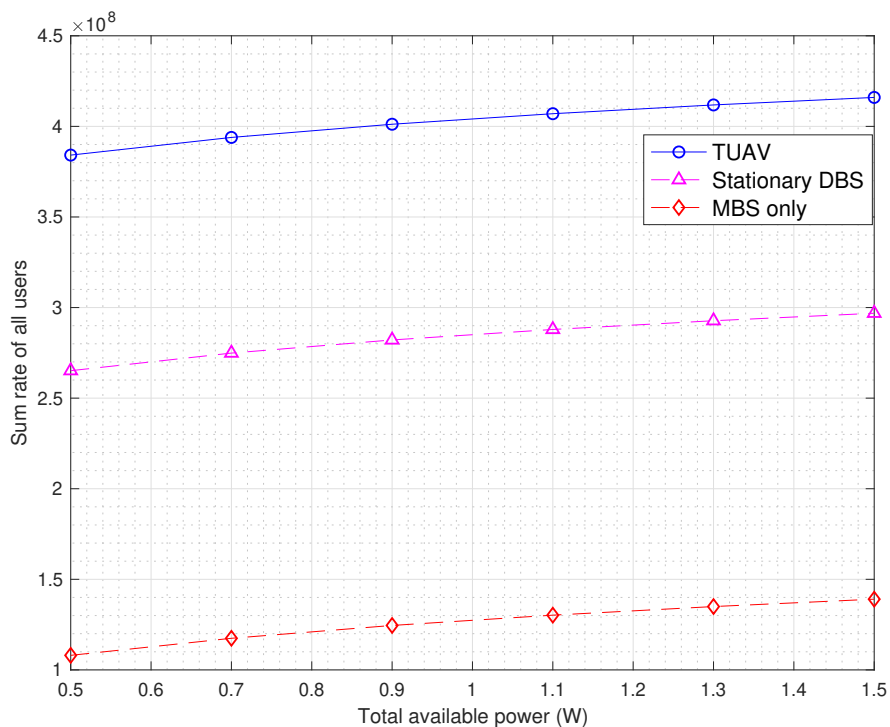**Figure 5.5** Sum rate of all users versus total available bandwidth.

**Figure 5.6** Sum rate of all users versus total available power.

Figures 5.5 and 5.6 illustrate the sum rate of all users versus the total available resource, i.e., the total available bandwidth and transmit power, respectively. It is observed that as the total available resource increases, the sum rate of all users increases in all three schemes. This is due to the fact that the sum rate is an increasing function of allocated bandwidth and transmit power. In addition, our proposed TUAV scheme achieves better performance as compared to the other two baseline algorithms. The rationale behind is that our proposed scheme can improve the sum rate of all users by adjusting the UAVs' locations (as compared with stationary DBS) and allocating more resource to the users which have better channel conditions (as compared with equal resource allocation). It is also observed that both schemes with relays outperform the MBS only scheme since better wireless channels are provided for the ground users as compared with directly connecting to the MBS.

Figures. 5.5 and 5.6 also show the gap between each scheme. For instance, given the total available bandwidth of 22MHz, the sum rates of the 'MBS only' scheme, the 'Stationary DBS' scheme and the proposed scheme are 132Mbps, 319Mbps and 422 Mbps, respectively. We can see that the sum rate of the users is increased by 141.7% by introducing a stationary DBS into an MBS only wireless network because the favorable Line of Sight (LoS) connection can be established between the users and the DBS. In comparison, the increase obtained from the 'Stationary DBS' scheme to the TUAV scheme is not as significant as the increase obtained from the 'MBS only' scheme to the 'Stationary DBS' scheme. This is because the 'Stationary DBS' scheme and the TUAV scheme share the same pathloss model and the gain is limited by adjusting the locations of the UAVs.

Furthermore, our proposed approach can theoretically provide unlimited time service to the users, while a DBS without charging can last for no more than 1 hour.

# CHAPTER 6

# FUTURE WORK

We have proposed to deploy a UAV to improve the system throughput and reduce the latency in Chapter 3 and Chapter 4, respectively. The UAV can effectively provision LoS communication links between the ground users and the MBS, thus improving the performance of existing cellular networks. In Chapter 5, to enable the UAVs to stay in the air for a longer time, we have proposed to connect the UAV with a ground charging station through a tether to provide the UAV with a stable power supply. In this chapter, we will briefly discuss how to solve the trajectory design problem (which is NP-hard) in UAV-enabled Internet of Things (IoT) Network by utilizing the deep reinforcement learning (DRL) method. Meanwhile, we will also introduce how to minimize the energy consumption of the UAV in a low Earth orbit (LEO) satellite-assisted UAV data collection for the Internet of Remote Things (IoRT) sensors.

## 6.1 Trajectory Design in UAV-enabled IoT Network by Utilizing the DRL Method

IoT has attracted increasing interest in applications such as public safety, environment monitoring, intelligent agriculture, smart homes and smart cities [49–54]. All these applications involve data collection for centralized processing with consideration of the limited computation power and on-board energy of the IoT nodes. However, the data collection suffers from lack of surrounding terrestrial communication infrastructures or bad channel conditions from the IoT nodes to the base stations (BSs) since the IoT nodes are usually deployed in remote areas.

As shown in Figure 6.1, UAV [55], with the advantage of high mobility and flexible deployment, is capable of moving close to the IoT nodes and establishing
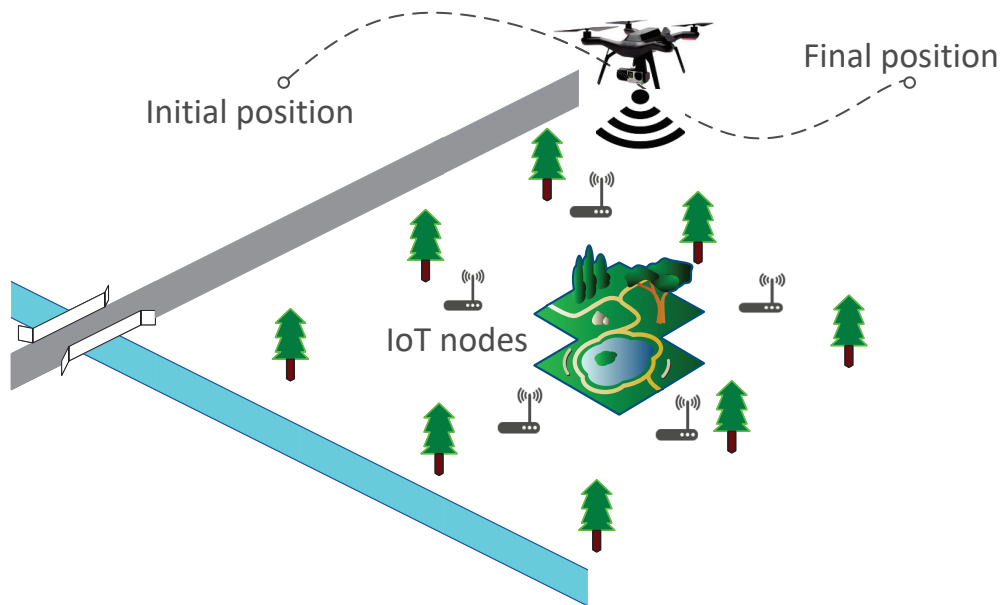
**Figure 6.1** The UAV-enabled IoT network.

the favorable LoS channels with a larger probability as it flies at a higher altitude as compared to the ground BSs. Hence, the UAV-enabled IoT is considered as a promising solution to address the above challenges. Through the design of the trajectory of the UAV and the association scheme, the ground IoT nodes can choose to transmit the data when the channel condition is better and thus greatly reduce the communication energy consumption.

One of the main challenges of UAV-enabled IoT network is the UAV trajectory design, regardless of the objective function (e.g., system throughput maximization, energy consumption minimization or completion time minimization). The formulated optimization problem is generally non-convex since the data rate is non-convex w.r.t. the UAV's location at each time slot. DRL has been proved to be an effective tool in solving problems which cannot be easily handled by traditional optimization methods [36,56]. Reinforcement learning, which learns while interacting with the environment [57,58], is capable of obtaining the near-optimal solution in a trial and error manner [59–63]. However, with the increase of the state space or action space, it is infeasible

to explore all states or actions. The artificial neural network, which approximates the optimal state-value function by minimizing the loss function (or the reward prediction error) [64], can generalize what it has learned from past experience. Once the learning procedure is finished, the weights of the neurons in each layer is fixed and can be applied to the applications. To obtain the near optimal solution of the completion time minimization problem in the UAV-enabled IoT network , we will investigate to jointly determine the UAV's trajectory and user association by utilizing the DRL method.

## 6.2 LEO Satellite-assisted UAV Data Collection for the IoRT Sensors

As shown in Figure 6.2, one of the main issues in 6G network is the integration of LEO satellite networks and terrestrial networks [65–67]. This new satellite architecture will revolutionize traditional communication networks with its promising benefits of service continuity, wide-area coverage, and availability for critical communications and emerging applications (e.g., Internet of Remote Things). However, it is still challenging to connect all the IoRT sensors with the LEO satellites directly considering the long distance and low transmission power of the IoRT sensors. Therefore, the delay sensitive data can be relayed by LEO satellite networks back to the ground MBSs. While the delay tolerant data can be collected by the UAVs in the carry-store mode for further processing. UAVs, with its high mobility and deployment flexibility, show great advantages in helping the integration of LEO satellite networks and terrestrial networks. UAVs can be classifed into two main categories: rotary wing and fxed wing. A rotary wing UAV can theoretically hover at a fxed location while a fxedwing UAV has to maintain a minimum speed to stay aloft in the air. Unfortunately, a rotary wing UAV generally consumes more energy and has less on-board energy as compared with a fxed-wing UAV. To guarantee the data collection
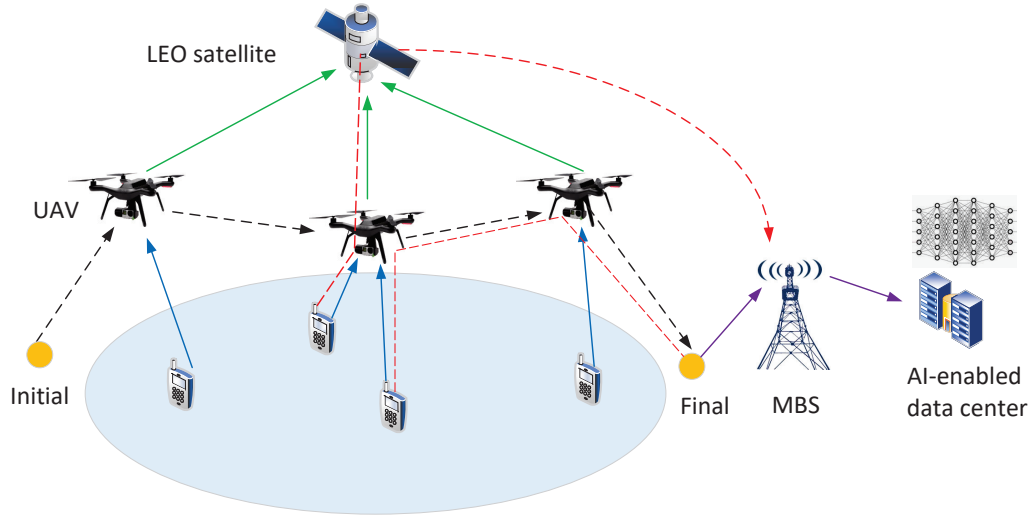
**Figure 6.2** LEO satellite-assisted UAV data collection .

completion, fxed-wing UAV which has more on-board energy possesses an apparent advantage over the rotary wing UAV.

Considering the limited on-board energy, it is critical to optimize the trajectory to minimize the propulsion energy consumption of the UAV while satisfying the delay requirements. The trajectory design (i.e., the location of the UAV at each time slot) directly determines the propulsion energy consumption of the UAV [68]. Moreover, an optimized bandwidth allocation scheme can also reduce energy consumption of the UAV by shortening the data offloading time such that the whole mission time can be reduced. Additionally, the association scheme of the IoRT sensors should also be carefully designed because the generated data may be delay sensitive or tolerant. Note that the trajectory design of the UAV, the resource allocation scheme and association policy of the IoRT sensors are mutually dependent. Hence, we should jointly consider these three subproblems to minimize the energy consumption of the UAV.

To solve the formulated energy minimization problem, we will investigate and design a block coordinate descent (BCD) based cyclic iterative algorithm which decomposes the joint optimization problem into three subproblems, i.e., the resource allocation problem, the trajectory design problem and the association problem. Since

the trajectory design problem is still non-convex and diffcult to solve, we plan to transform it into a convex optimization problem by leveraging the successive convex approximation (SCA) technique. The iterative algorithm is stopped when no further performance improvement can be achieved or the maximum allowed number of iterations is reached.

# CHAPTER 7

# CONCLUSION

We have studied the resource allocation, user association and placement in UAV-assisted communications to improve the performance of existing cellular networks. First, we proposed to deploy a UAV over a given area with FSO-based backhaul to increase the system throughput. We have formulated an optimization problem to maximize the capacity in the access link subject to the user QoS requirements and limited available resource. To solve the problem, we designed a Cyclic Iterative UAV placEment and Resource allocation (CIDER) algorithm to decompose the primal problem into two subproblems and then solved the two sub-problems separately. Second, we studied the latency minimization in UAV-assisted heterogeneous networks with FSO working as the backhaul link. Intuitively, more users should be associated with the UAV since an LoS communication link is more likely to be established between the DBS and a user. However, too many users associating with the UAV may increase the traffic load and thus significantly increase the latency ratio of the users. Therefore, we tried to minimize the average latency ratio of all users with the constraint of each user's QoS requirement and total available bandwidth. To make the formulated problem more tractable, we decomposed it into two subproblems and optimized them iteratively by using the output of one as the input for the other. Numerical simulation results demonstrated the significant latency ratio reduction achieved by our proposed algorithm as compared to other baseline schemes. Third, to prolong the lifetime of the UAV, we proposed o connect the UAV through a tether with a GCS. The GCS can provide a stable power supply while maintaining UAV's maneuverability to a certain extent. Different from deploying untethered UAVs, deploying multiple TUAVs may cause tangling among them or tangling with the

surrounding buildings. Furthermore, the TUAV placement problem involves not only the placement of the aerial UAVs but also that of the GCSs. To address the above challenges, we proposed a Cyclic iterAtive TUAV placeMent, usEr association and Resource Allocation (CAMERA) algorithm to maximize the sum rate in the access link with the constraints of limited available resource, tangling avoidance and user QoS requirements. Numerical experiments have demonstrated that our proposed algorithm outperforms baseline algorithms under different setups. We have further delineated two future research endeavors: 1) trajectory design in UAV-enabled IoT network by leveraging deep reenforcement learning, and 2) LEO satellite-assisted UAV data collection for the IoRT sensors.

# REFERENCES

[1] M. Mozaffari, W. Saad, M. Bennis, and M. Debbah, "Unmanned aerial vehicle with underlaid device-to-device communications: Performance and tradeoffs," *IEEE Transactions on Wireless Communications*, vol. 15, no. 6, pp. 3949–3963, 2016.

[2] X. Sun, N. Ansari, and R. Fierro, "Jointly optimized 3D drone mounted base station deployment and user association in drone assisted mobile access networks," *IEEE Transactions on Vehicular Technology*, vol. 69, no. 2, pp. 2195–2203, 2020.

[3] A. Al-Hourani, S. Kandeepan, and S. Lardner, "Optimal LAP altitude for maximum coverage," *IEEE Wireless Communications Letters*, vol. 3, no. 6, pp. 569–572, 2014.

[4] S. Zhang and N. Ansari, "3D drone base station placement and resource allocation with fso-based backhaul in hotspots," *IEEE Transactions on Vehicular Technology*, vol. 69, no. 3, pp. 3322–3329, 2020.

[5] A. K. Majumdar, "Free-space laser communication performance in the atmospheric channel," *Journal of Optical and Fiber Communications Reports*, vol. 2, no. 4, pp. 345–396, 2005.

[6] H. E. Nistazakis, T. A. Tsiftsis, and G. S. Tombras, "Performance analysis of free-space optical communication systems over atmospheric turbulence channels," *IET Communications*, vol. 3, no. 8, pp. 1402–1409, 2009.

[7] T. Zhang, X. Sun, and C. Wang, "On optimizing the divergence angle of an FSO-based fronthaul link in drone-assisted mobile networks," *IEEE Internet of Things Journal*, vol. 9, no. 9, pp. 6914–6921, 2022.

[8] I. I. Kim, B. McArthur, and E. J. Korevaar, "Comparison of laser beam propagation at 785 nm and 1550 nm in fog and haze for optical wireless communications," in *Optical Wireless Communications III*, vol. 4214. SPIE, 2001, pp. 26–37.

[9] D. Wu, X. Sun, and N. Ansari, "An FSO-based drone assisted mobile access network for emergency communications," *IEEE Transactions on Network Science and Engineering*, vol. 7, no. 3, pp. 1597–1606, 2020.

[10] S. Zhang and N. Ansari, "Latency aware 3D placement and user association in drone-assisted heterogeneous networks with FSO-based backhaul," *IEEE Transactions on Vehicular Technology*, vol. 70, no. 11, pp. 11 991–12 000, 2021.

[11] S. Zhang, W. Liu, and N. Ansari, "On tethered uav-assisted heterogeneous network," *IEEE Transactions on Vehicular Technology*, vol. 71, no. 1, pp. 975–983, 2022.

[12] C.-X. Zu and H. Li, "Thermodynamic analysis on energy densities of batteries," *Energy & Environmental Science*, vol. 4, no. 8, pp. 2614–2624, 2011.

[13] X. Lu, P. Wang, D. Niyato, D. I. Kim, and Z. Han, "Wireless charging technologies: Fundamentals, standards, and network applications," *IEEE Communications Surveys & Tutorials*, vol. 18, no. 2, pp. 1413–1452, 2015.

[14] W. Liu, S. Zhang, and N. Ansari, "Joint laser charging and DBS placement for drone-assisted edge computing," *IEEE Transactions on Vehicular Technology*, vol. 71, no. 1, pp. 780–789, 2022.

[15] N. Ansari, Q. Fan, X. Sun, and L. Zhang, "SoarNet," *IEEE Wireless Communications*, vol. 26, no. 6, pp. 37–43, 2019.

[16] D. Wu and N. Ansari, "A cooperative computing strategy for blockchain-secured fog computing," *IEEE Internet of Things Journal*, vol. 7, no. 7, pp. 6603–6609, 2020.

[17] E. Kalantari, M. Z. Shakir, H. Yanikomeroglu, and A. Yongacoglu, "Backhaul-aware robust 3d drone placement in 5g+ wireless networks," in *2017 IEEE International Conference on Communications Workshops (ICC Workshops)*. IEEE, 2017, pp. 109–114.

[18] X. Liu and N. Ansari, "Resource allocation in UAV-assisted M2M communications for disaster rescue," *IEEE Wireless Communications Letters*, vol. 8, no. 2, pp. 580–583, 2019.

[19] Y. Zeng, R. Zhang, and T. J. Lim, "Throughput maximization for uav-enabled mobile relaying systems," *IEEE Transactions on Communications*, vol. 64, no. 12, pp. 4983–4996, 2016.

[20] L. Xie, J. Xu, and R. Zhang, "Throughput maximization for uav-enabled wireless powered communication networks," *IEEE Internet of Things Journal*, vol. 6, no. 2, pp. 1690–1703, 2018.

[21] C. Zhan, H. Hu, X. Sui, Z. Liu, and D. Niyato, "Completion time and energy optimization in the uav-enabled mobile-edge computing system," *IEEE Internet of Things Journal*, vol. 7, no. 8, pp. 7808–7822, 2020.

[22] Z. M. Fadlullah, D. Takaishi, H. Nishiyama, N. Kato, and R. Miura, "A dynamic trajectory control algorithm for improving the communication throughput and delay in uav-aided networks," *IEEE Network*, vol. 30, no. 1, pp. 100–105, 2016.

[23] D. Takaishi, Y. Kawamoto, H. Nishiyama, N. Kato, F. Ono, and R. Miura, "Virtual cell based resource allocation for efficient frequency utilization in unmanned aircraft systems," *IEEE Transactions on Vehicular Technology*, vol. 67, no. 4, pp. 3495–3504, 2017.

[24] M. Najafi, H. Ajam, V. Jamali, P. D. Diamantoulakis, G. K. Karagiannidis, and R. Schober, "Statistical modeling of fso fronthaul channel for drone-based networks," in *2018 IEEE International Conference on Communications (ICC)*. IEEE, 2018, pp. 1–7.

[25] M. Alzenad, M. Z. Shakir, H. Yanikomeroglu, and M.-S. Alouini, "Fso-based vertical backhaul/fronthaul framework for 5g+ wireless networks," *IEEE Communications Magazine*, vol. 56, no. 1, pp. 218–224, 2018.

[26] A. A. Farid and S. Hranilovic, "Outage capacity optimization for free-space optical links with pointing errors," *Journal of Lightwave technology*, vol. 25, no. 7, pp. 1702–1710, 2007.

[27] M. A. Kishk, A. Bader, and M.-S. Alouini, "On the 3-d placement of airborne base stations using tethered uavs," *IEEE Transactions on Communications*, vol. 68, no. 8, pp. 5202–5215, 2020.

[28] P. Sudheesh, M. Mozaffari, M. Magarini, W. Saad, and P. Muthuchidambaranathan, "Sum-rate analysis for high altitude platform (hap) drones with tethered balloon relay," *IEEE Communications Letters*, vol. 22, no. 6, pp. 1240–1243, 2017.

[29] A. Alzidaneen, A. Alsharoa, and M.-S. Alouini, "Resource and placement optimization for multiple uavs using backhaul tethered balloons," *IEEE Wireless Communications Letters*, vol. 9, no. 4, pp. 543–547, 2019.

[30] V. U. Pai and B. Sainath, "Uav selection and link switching policy for hybrid tethered uav-assisted communication," *IEEE Communications Letters*, vol. 25, no. 7, pp. 2410–2414, 2021.

[31] S. Zhang, X. Sun, and N. Ansari, "Placing multiple drone base stations in hotspots," in *IEEE 39th Sarnoff Symposium*, Newark, NJ, 2018, pp. 1–6.

[32] A. Al-Hourani, S. Kandeepan, and A. Jamalipour, "Modeling air-to-ground path loss for low altitude platforms in urban environments," in *IEEE Global Communications Conference*, Austin, Texas, Dec. 2014, pp. 2898–2904.

[33] J. Yao and N. Ansari, "Online task allocation and flying control in fog-aided internet of drones," *IEEE Transactions on Vehicular Technology*, vol. 69, no. 5, pp. 5562–5569, May 2020.

[34] M. Alzenad, A. El-Keyi, and H. Yanikomeroglu, "3-d placement of an unmanned aerial vehicle base station for maximum coverage of users with different qos requirements," *IEEE Wireless Communications Letters*, vol. 7, no. 1, pp. 38–41, 2017.

[35] M. Alzenad, A. El-Keyi, F. Lagum, and H. Yanikomeroglu, "3-d placement of an unmanned aerial vehicle base station (uav-bs) for energy-efficient maximal coverage," *IEEE Wireless Communications Letters*, vol. 6, no. 4, pp. 434–437, 2017.

[36] S. Boyd and L. Vandenberghe, *Convex Optimization*. Cambridge: Cambridge University Press, 2004.

[37] L. Jeinroek, *Queueing Systems Vol. 2: Computer Applications*. NewYork: Wiley, 1976.

[38] X. Sun and N. Ansari, "Latency aware drone base station placement in heterogeneous networks," in *IEEE Global Communications Conference*. IEEE, 2017, pp. 1–6.

[39] H. Benson, "Global optimization algorithm for the nonlinear sum of ratios problem," *Journal of Optimization Theory and Applications*, vol. 112, no. 1, pp. 1–29, 2002.

[40] J. Yao and N. Ansari, "Qos-aware power control in internet of drones for data collection service," *IEEE Transactions on Vehicular Technology*, vol. 68, no. 7, pp. 6649–6656, 2019.

[41] Y. Jong, "Practical global optimization algorithm for the sum-of-ratios problem," *arXiv preprint arXiv:1207.1153*, 2012.

[42] J. B. Rosen, "The gradient projection method for nonlinear programming. part i. linear constraints," *Journal of the Society for Industrial and Applied Mathematics*, vol. 8, no. 1, pp. 181–217, 1960.

[43] Q. Wu, Y. Zeng, and R. Zhang, "Joint trajectory and communication design for multi-uav enabled wireless networks," *IEEE Transactions on Wireless Communications*, vol. 17, no. 3, pp. 2109–2121, 2018.

[44] M. Haenggi, *Stochastic geometry for wireless networks*. New York, NY, USA: Cambridge University Press, 2012.

[45] R. K. Ganti and M. Haenggi, "Interference and outage in clustered wireless ad hoc networks," *IEEE Transactions on Information Theory*, vol. 55, no. 9, pp. 4067–4086, 2009.

[46] D. P. Bertsekas and J. N. Tsitsiklis, *Parallel and Distributed Computation: Numerical Methods*. Prentice hall Englewood Cliffs, NJ, 1989, vol. 23.

[47] D. P. Bertsekas, *Nonlinear Programming*. Boston, MA: Athena, 1999.

[48] S. Martello and P. Toth, *Knapsack problems: algorithms and computer implementations*. Chichester, U.K.: John Wiley & Sons, Inc., 1990.

[49] A. Zanella, N. Bui, A. Castellani, L. Vangelista, and M. Zorzi, "Internet of things for smart cities," *IEEE Internet of Things journal*, vol. 1, no. 1, pp. 22–32, 2014.

[50] M. Ayaz, M. Ammad-Uddin, Z. Sharif, A. Mansour, and E.-H. M. Aggoune, "Internet-of-things (iot)-based smart agriculture: Toward making the fields talk," *IEEE Access*, vol. 7, pp. 129 551–129 583, 2019.

[51] L. Da Xu, W. He, and S. Li, "Internet of things in industries: A survey," *IEEE Transactions on Industrial Informatics*, vol. 10, no. 4, pp. 2233–2243, 2014.

[52] X. Liu and N. Ansari, "Profit-driven user association and smart grid energy transfer in green cellular networks," *IEEE Transactions on Vehicular Technology*, vol. 68, no. 10, pp. 10 111–10 120, 2019.

[53] X. Sun and N. Ansari, "Edgeiot: Mobile edge computing for the Internet of Things," *IEEE Communications Magazine*, vol. 54, no. 12, pp. 22–29, 2016.

[54] X. Liu and N. Ansari, "Toward green IoT: Energy solutions and key challenges," *IEEE Communications Magazine*, vol. 57, no. 3, pp. 104–110, 2019.

[55] J. Gundlach, *Designing Unmanned Aircraft Systems: A Comprehensive Approach.* Reston, VA, USA: American Institute of Aeronautics and Astronautics, 2012.

[56] M. Neely, *Stochastic Network Optimization with Application to Communication and Queueing Systems.* San Rafael, CA, USA: Morgan & Claypool, 2010.

[57] H. Xu, J. Wu, J. Li, and X. Lin, "Deep-reinforcement-learning-based cybertwin architecture for 6g iiot: An integrated design of control, communication, and computing," *IEEE Internet of Things Journal*, vol. 8, no. 22, pp. 16 337–16 348, 2021.

[58] R. Ali, I. Ashraf, A. K. Bashir, and Y. B. Zikria, "Reinforcement-learning-enabled massive internet of things for 6g wireless communications," *IEEE Communications Standards Magazine*, vol. 5, no. 2, pp. 126–131, 2021.

[59] V. Mnih, K. Kavukcuoglu, D. Silver, A. A. Rusu, J. Veness, M. G. Bellemare, A. Graves, M. Riedmiller, A. K. Fidjeland, G. Ostrovski *et al.*, "Human-level control through deep reinforcement learning," *Nature*, vol. 518, no. 7540, pp. 529–533, 2015.

[60] R. S. Sutton and A. G. Barto, *Reinforcement learning: An introduction.* Cambridge, MA: MIT press, 2018.

[61] M. L. Puterman, *Markov Decision Processes: Discrete Stochastic Dynamic Programming.* New York: John Wiley & Sons, 2014.

[62] T. P. Lillicrap, J. J. Hunt, A. Pritzel, N. Heess, T. Erez, Y. Tassa, D. Silver, and D. Wierstra, "Continuous control with deep reinforcement learning," *arXiv preprint arXiv:1509.02971*, 2015.

[63] V. Mnih, K. Kavukcuoglu, D. Silver, A. Graves, I. Antonoglou, D. Wierstra, and M. Riedmiller, "Playing atari with deep reinforcement learning," *arXiv preprint arXiv:1312.5602*, 2013.

[64] J. Schulman, F. Wolski, P. Dhariwal, A. Radford, and O. Klimov, "Proximal policy optimization algorithms," *arXiv preprint arXiv:1707.06347*, 2017.

[65] T. Darwish, G. K. Kurt, H. Yanikomeroglu, M. Bellemare, and G. Lamontagne, "Leo satellites in 5g and beyond networks: A review from a standardization perspective," *arXiv preprint arXiv:2110.08654*, 2021.

[66] Z. Jia, M. Sheng, J. Li, D. Niyato, and Z. Han, "Leo-satellite-assisted uav: Joint trajectory and data collection for internet of remote things in 6g aerial access networks," *IEEE Internet of Things Journal*, vol. 8, no. 12, pp. 9814–9826, 2020.

[67] A. Alsharoa and M.-S. Alouini, "Improvement of the global connectivity using integrated satellite-airborne-terrestrial networks with resource optimization," *IEEE Transactions on Wireless Communications*, vol. 19, no. 8, pp. 5088–5100, 2020.

[68] Y. Zeng and R. Zhang, "Energy-efficient UAV communication with trajectory optimization," *IEEE Trans. Wireless Commun.*, vol. 16, no. 6, pp. 3747–3760, Jun. 2017.